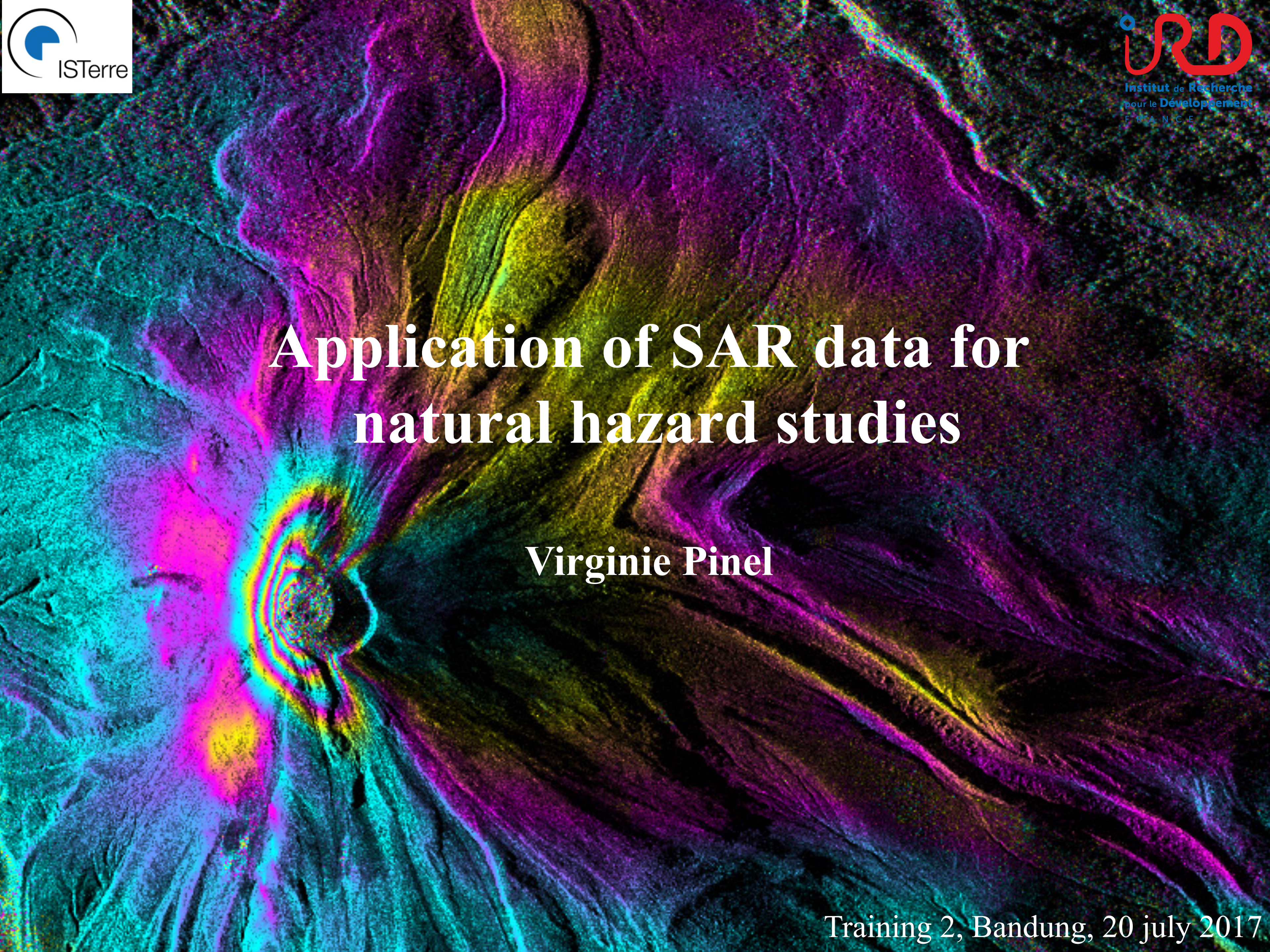

ISTerre

Institut de Recherche pour le Développement
FRANCE

Application of SAR data for natural hazard studies

Virginie Pinel

Training 2, Bandung, 20 july 2017

Who I am:

<u>Virginie Pinel</u>: Research Scientist at IRD
Virginie.Pinel@ird.fr

I work at Chambéry (France)

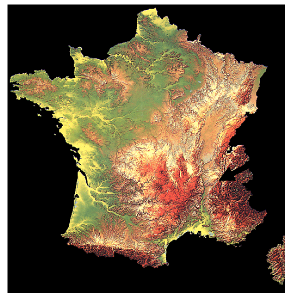

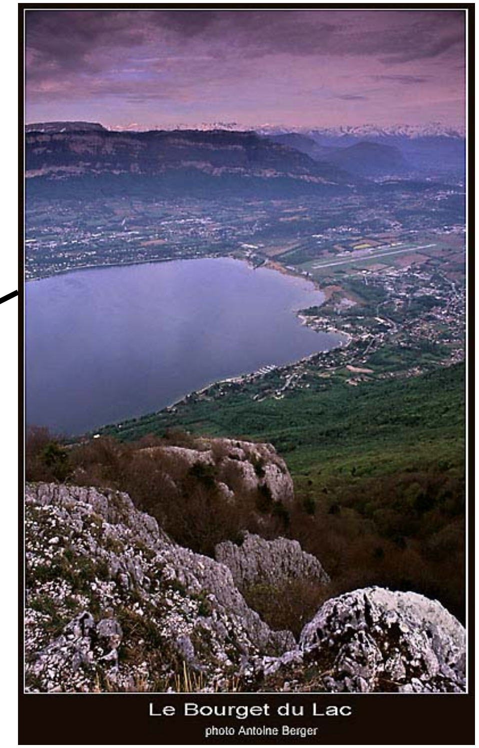

Magma storage and transport through the crust

-Deformation study by InSAR
-Modeling (analytical + numerical) of magmatic plumbing systems beneath volcanoes

You can download this presentation on my web page.
http://isterre.fr/staff-directory/member-web-pages/virginie-pinel/

SAR application summary

- Production of surface displacement field maps:
  - Earthquakes (co-seismic)
  - Inter-seismic loading on faults
  - Landslides
  - Volcanoes
  - *Subsidence in urban areas*
- DEM production
- Detection of surface changes
  - Estimation of post-event damages
  - Mapping of eruptive deposits

SAR application summary

- Production of surface displacement field maps:
  - Earthquakes (co-seismic)
  - Inter-seismic loading on faults
  - Landslides
  - Volcanoes
  - *Subsidence in urban areas*
- DEM production
- Detection of surface changes
  - Estimation of post-event damages
  - Mapping of eruptive deposits

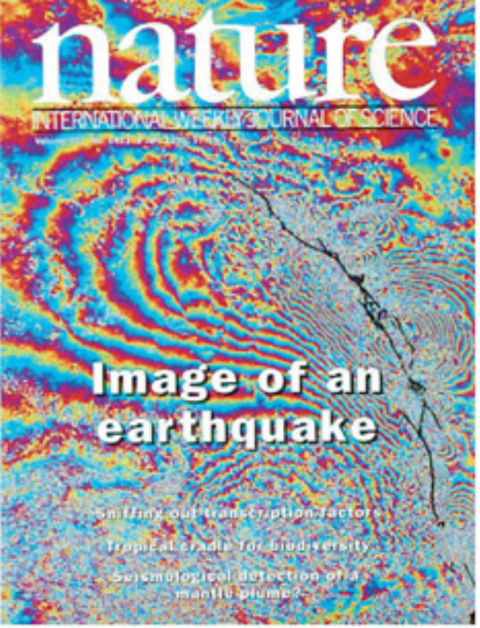

Landers Earthquake, California, USA, 1992, Mw 7.3

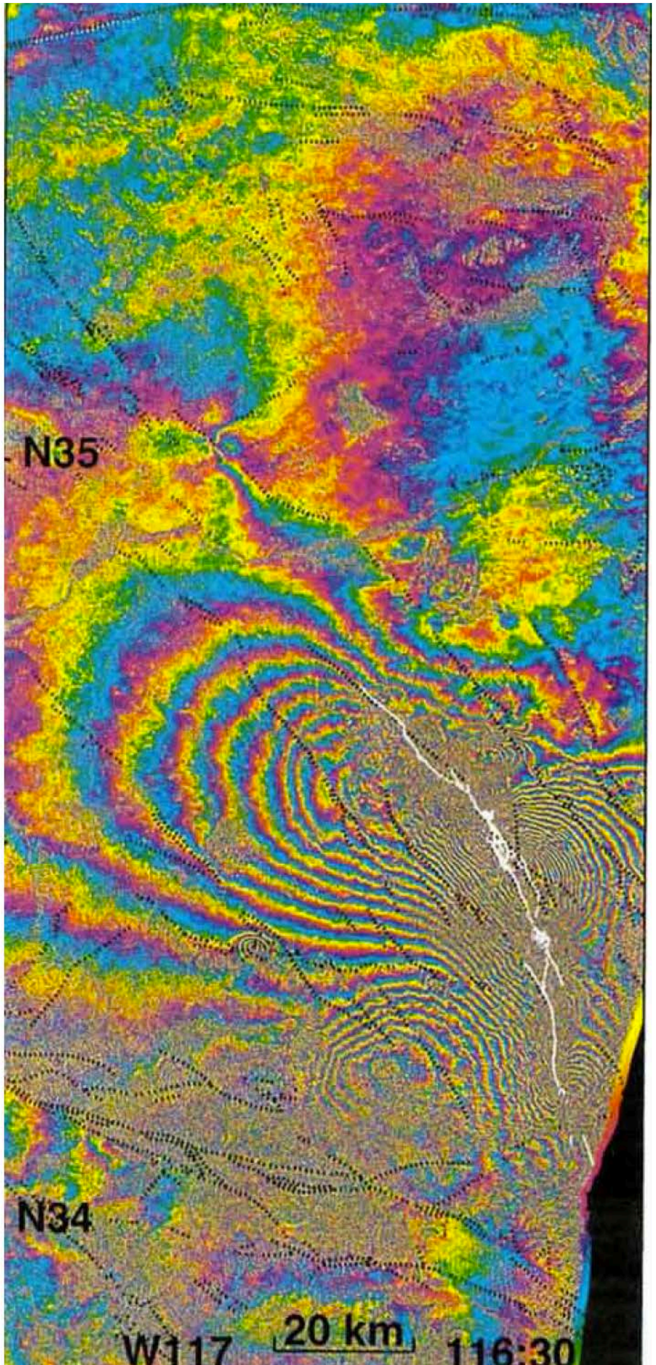

Massonnet et al, Nature 1993

Earthquake displacement field

- Kashmir earthquake (M_w=7.6) of October 8, 2005

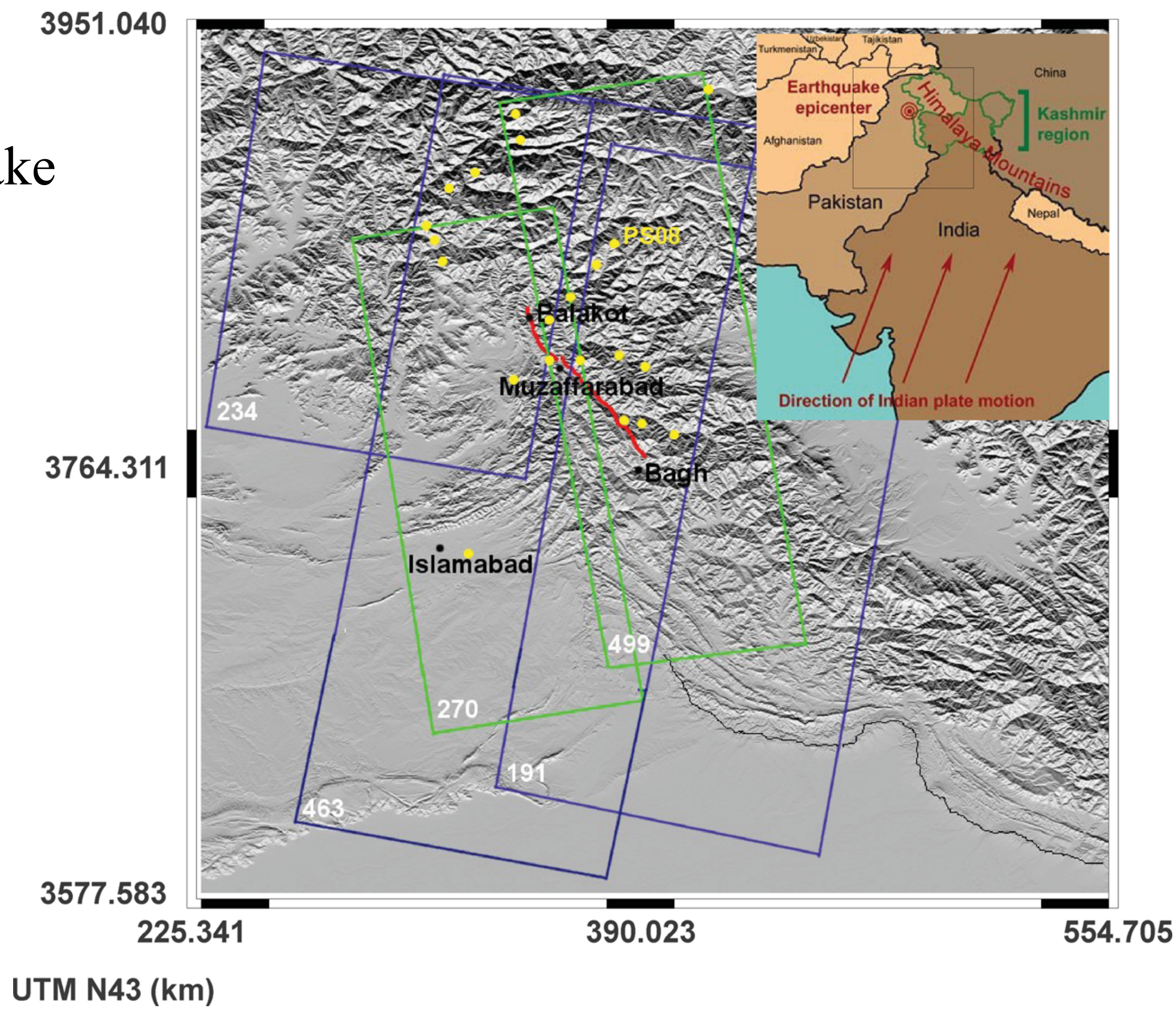

From Yan et al, 2013

Earthquake displacement field

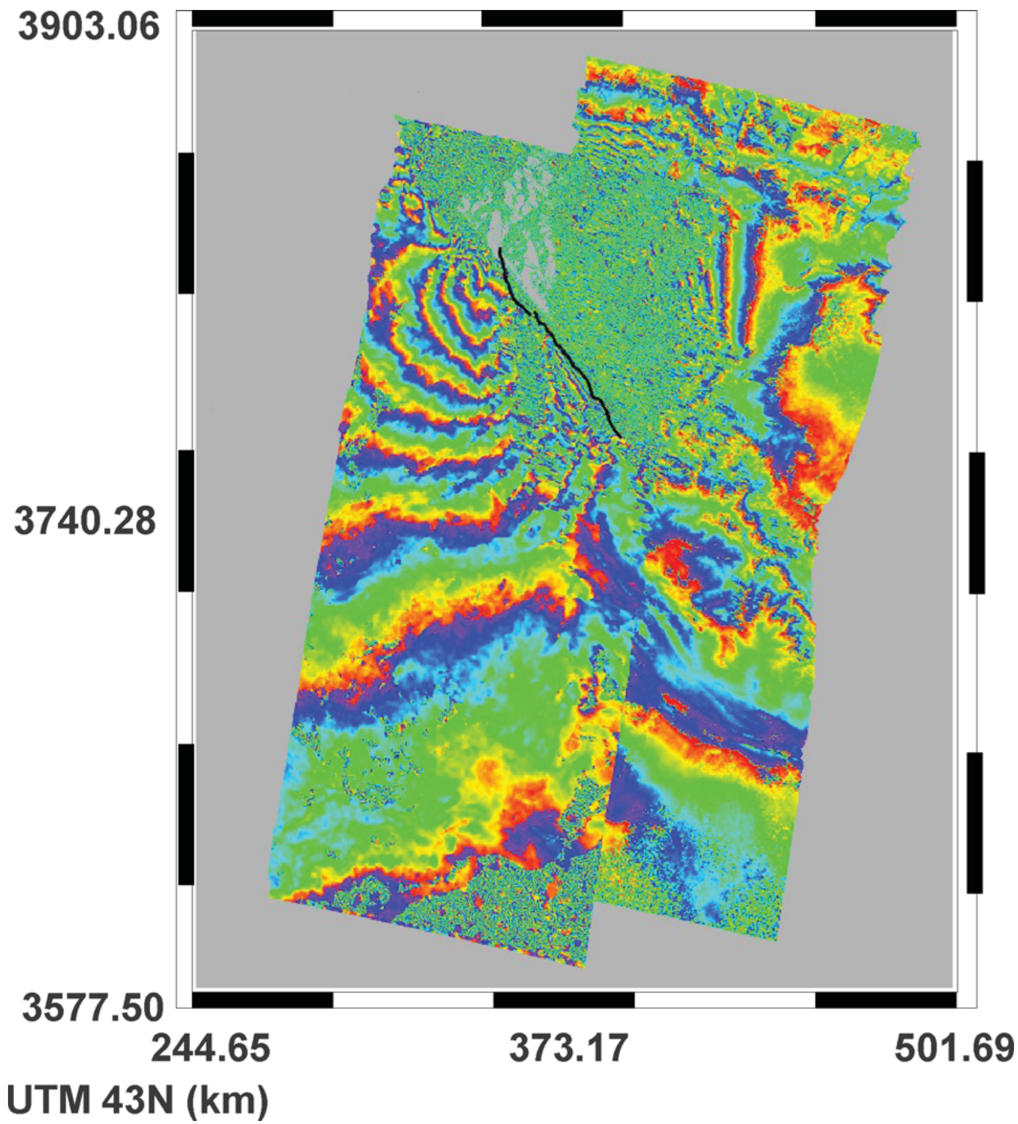

From Yan et al, 2013

Earthquake displacement field

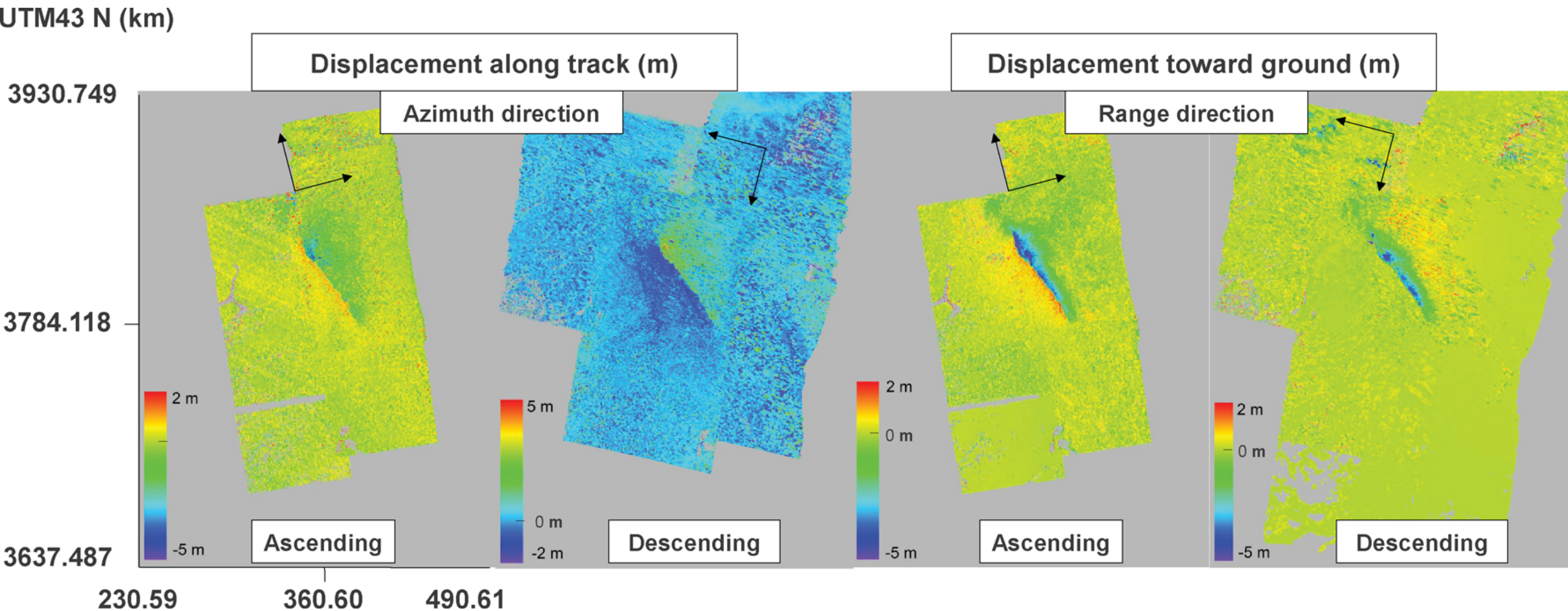

Coseismic displacement field obtained by fusion of subpixel image correlation and D-InSAR measurements. The location of each track is shown in
Fig. 1. For each pixel, the displacement value corresponds to the displacement value whose associated uncertainty is the smallest among all of the available measurements. The colour discontinuity corresponds to the fault rupture.

From Yan et al, 2013

Earthquake displacement field

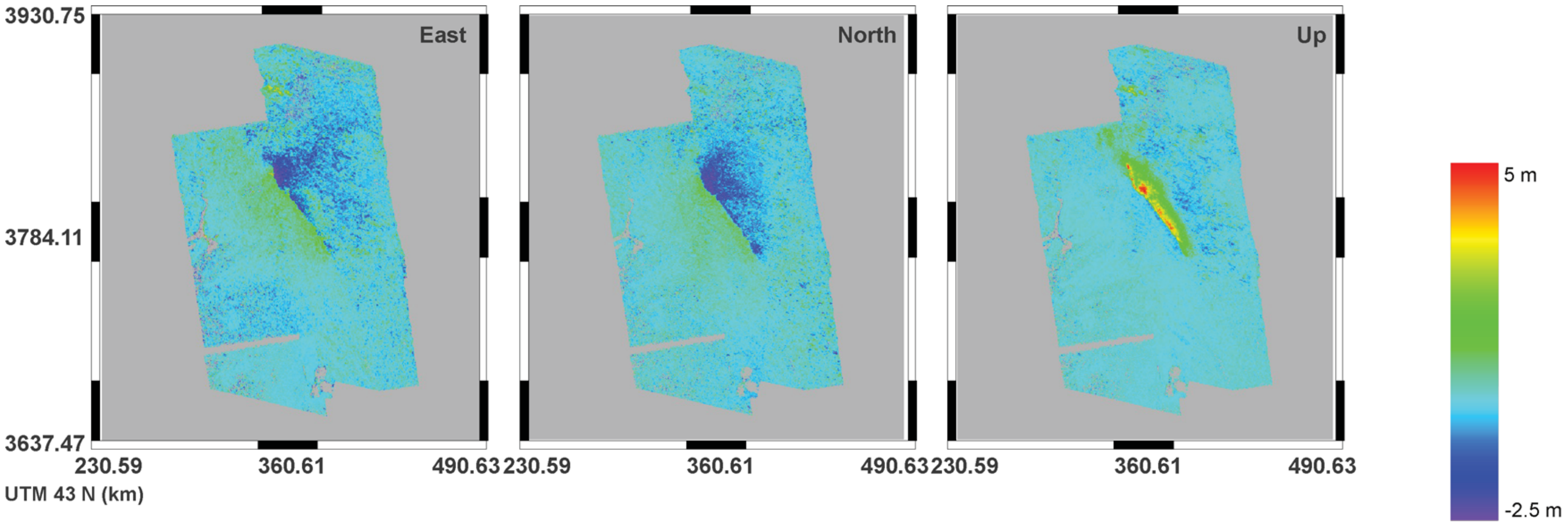

From Yan et al, 2013

Earthquake displacement field

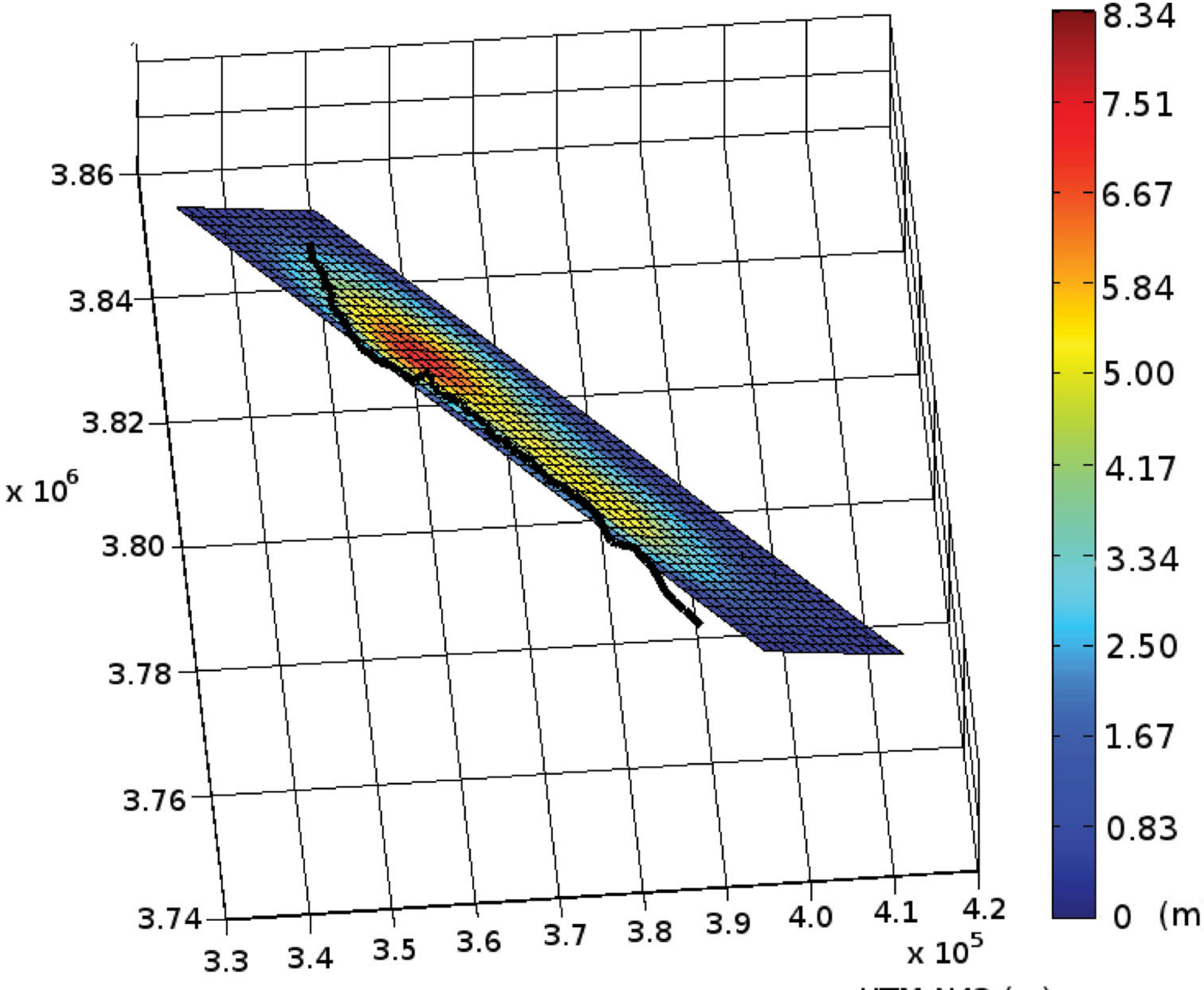

From Yan et al, 2013

Earthquake displacement field

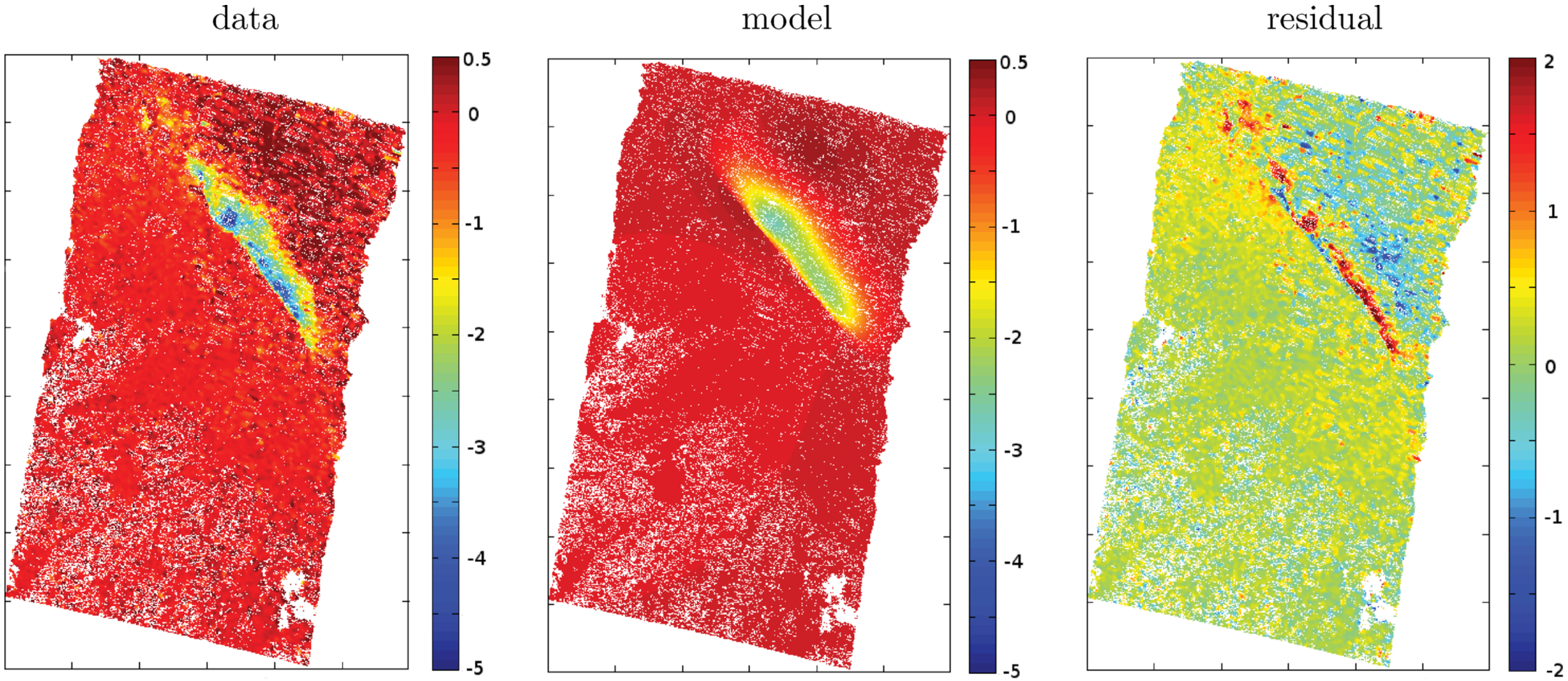

(a)

From Yan et al, 2013

Earthquake displacement field

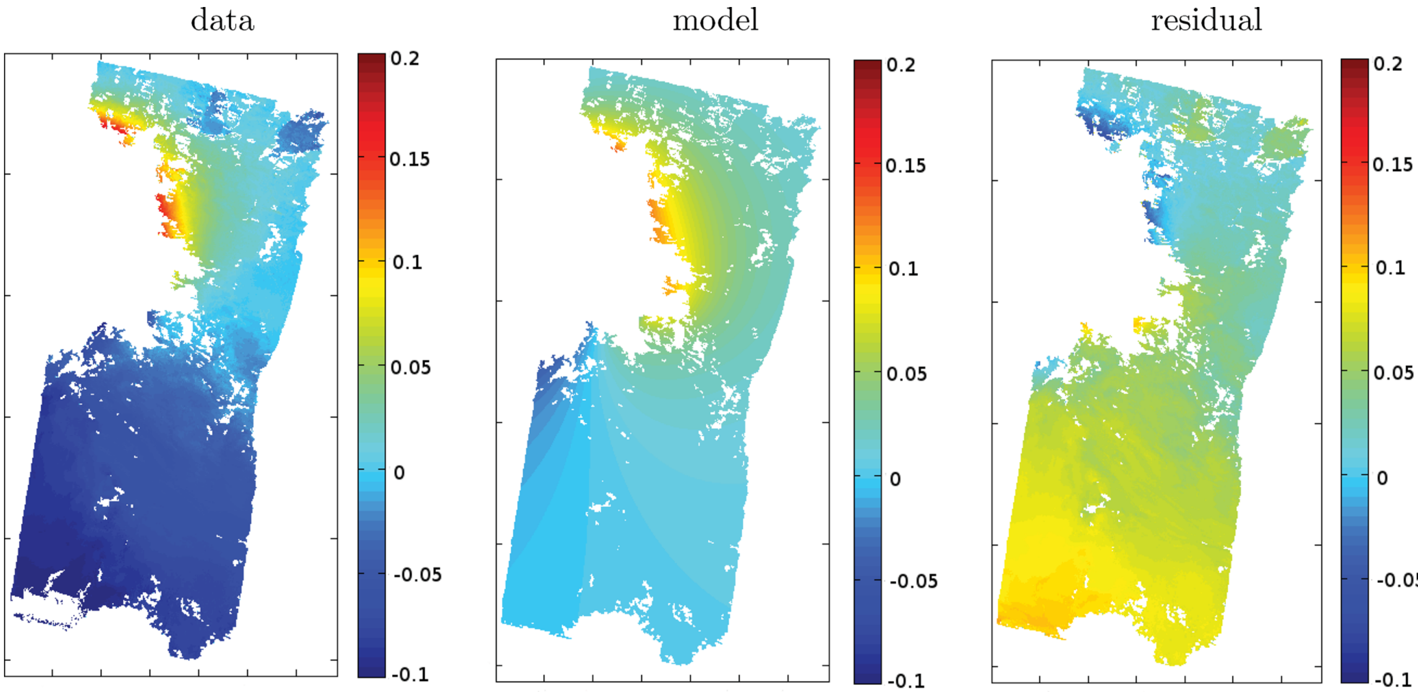

(a)

From Yan et al, 2013

SAR application summary

- Production of surface displacement field maps:
  - Earthquakes (co-seismic)
  - Inter-seismic loading on faults
  - Landslides
  - Volcanoes
  - *Subsidence in urban areas*
- DEM production
- Detection of surface changes
  - Estimation of post-event damages
  - Mapping of eruptive deposits

Interseismic velocity
Detection of slow aseismic slip

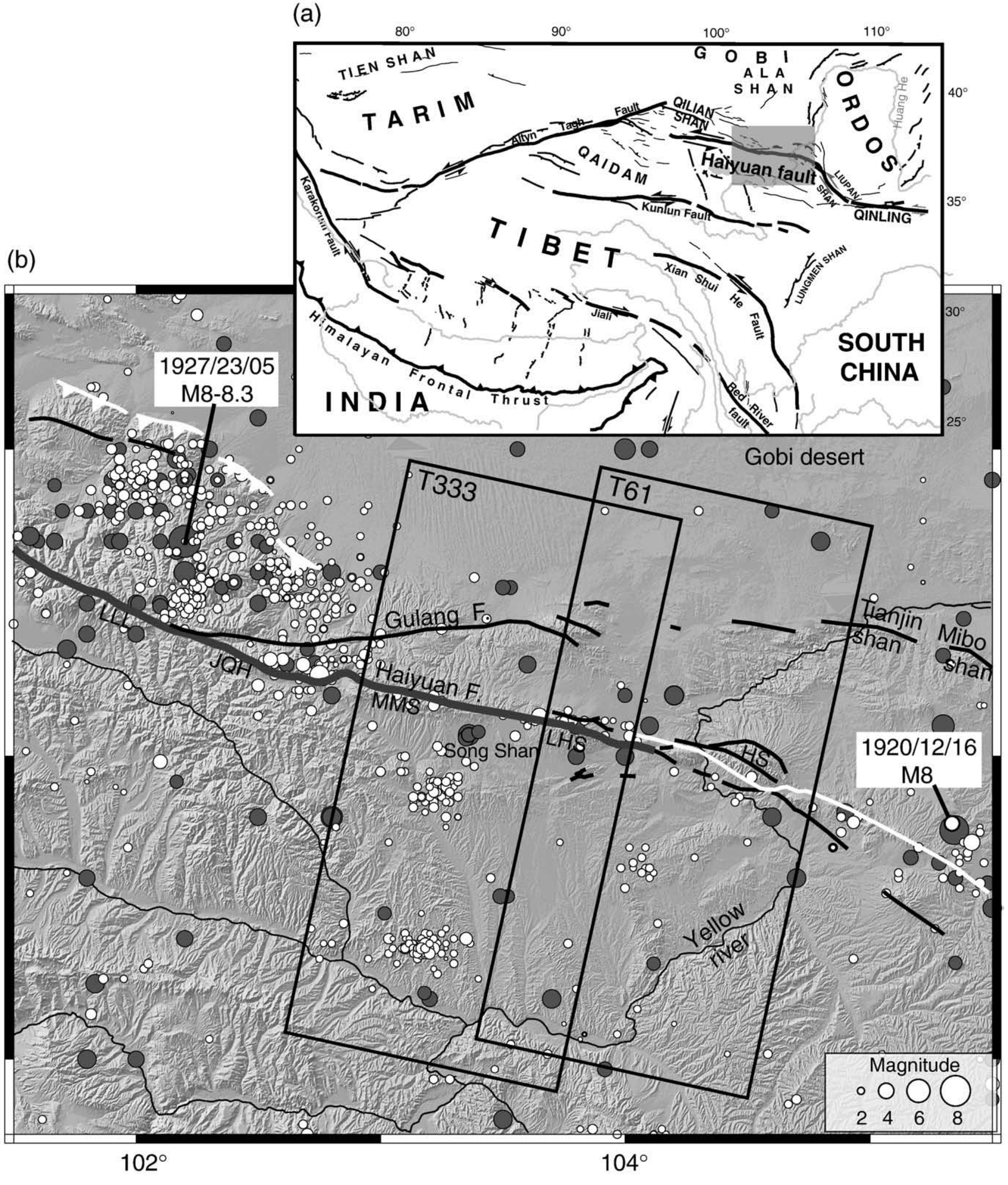

Haiyuan Fault, China
Shallow creep

(Cavalié et al., 2008)

Interseismic velocity
Detection of slow aseismic slip

Haiyuan Fault, China
Shallow creep

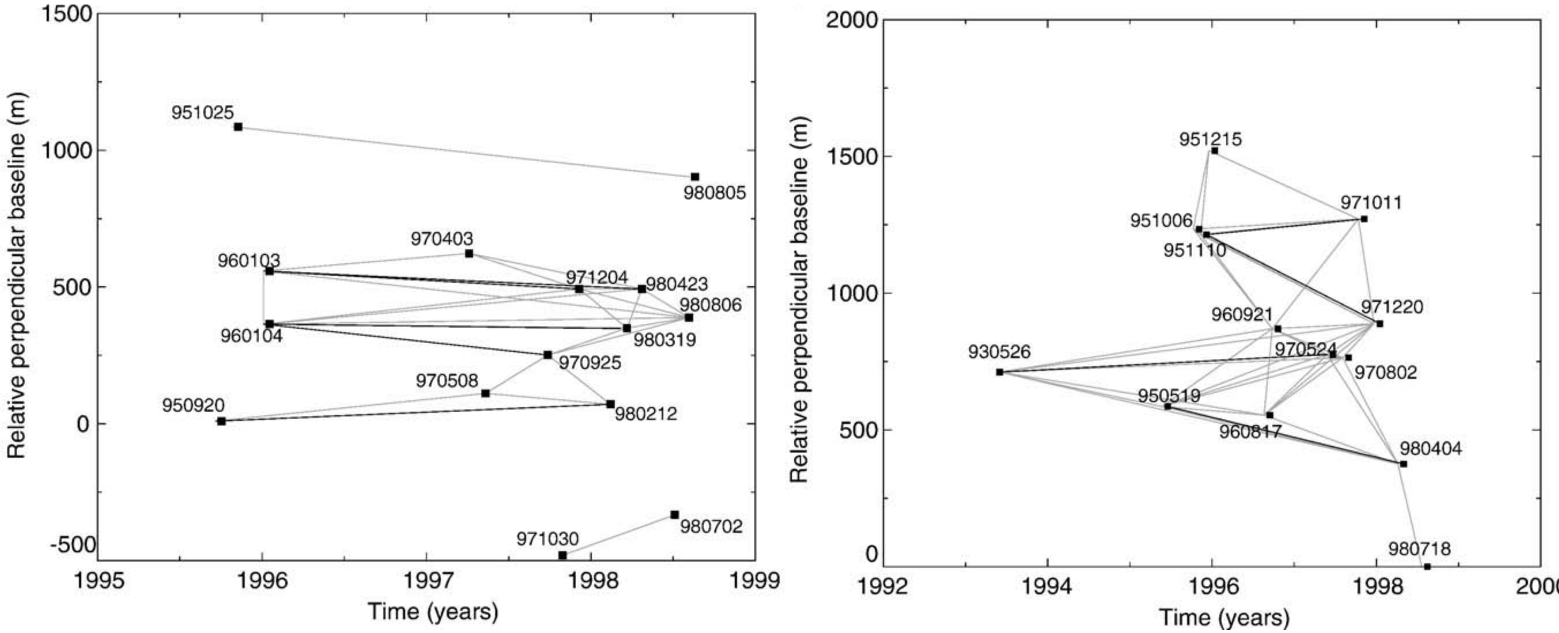

Track 333 Track 61

(Cavalié et al., 2008)

Interseismic velocity
Detection of slow aseismic slip

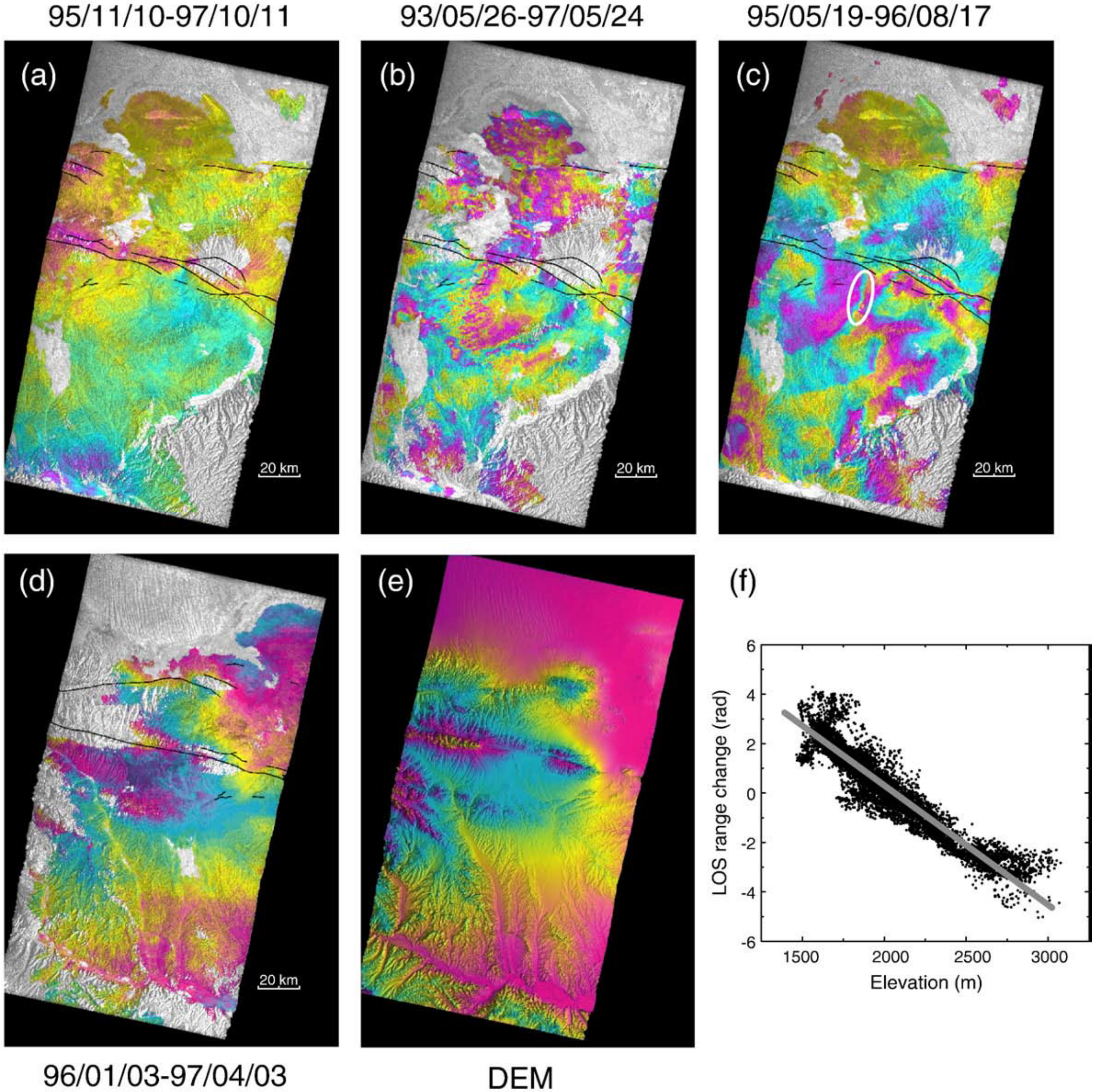

(Cavalié et al., 2008)

Interseismic velocity
Detection of slow aseismic slip

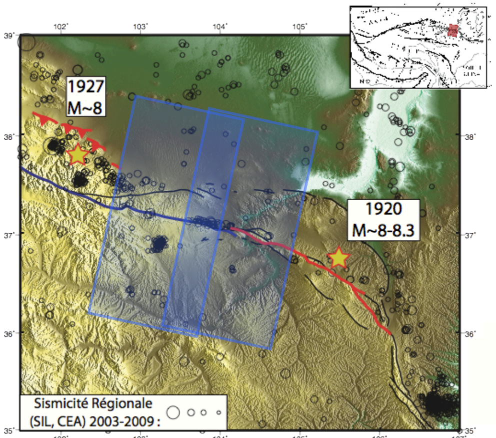

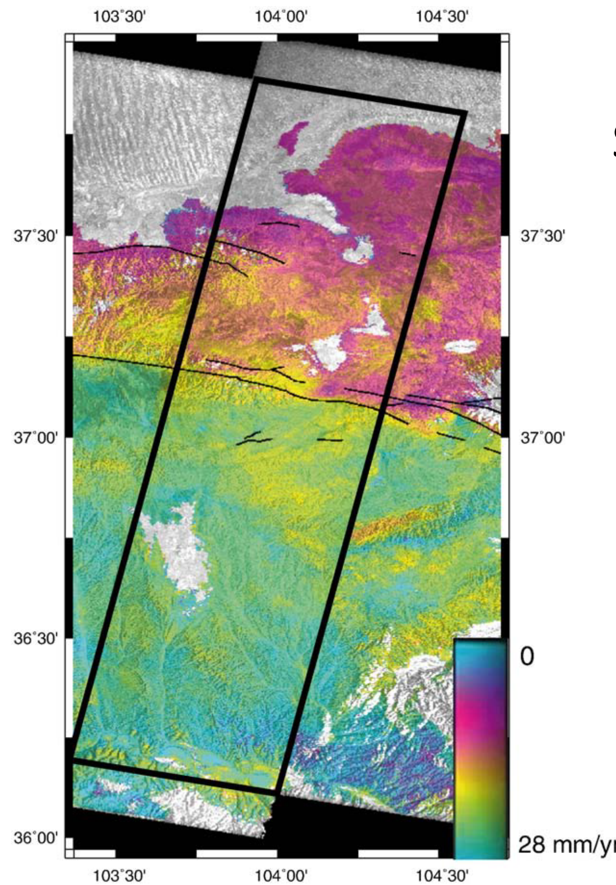

Haiyuan Fault, China
Shallow creep

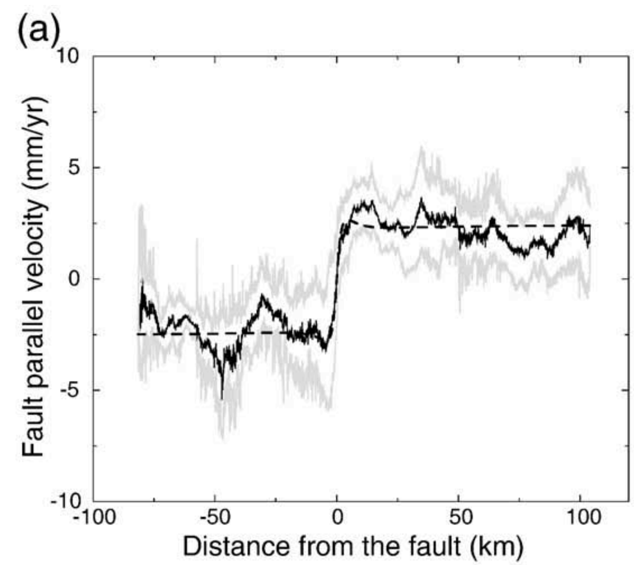

(Cavalié et al., 2008)

SAR application summary

- Production of surface displacement field maps:
  - Earthquakes (co-seismic)
  - Inter-seismic loading on faults
  - Landslides
  - Volcanoes
  - *Subsidence in urban areas*
- DEM production
- Detection of surface changes
  - Estimation of post-event damages
  - Mapping of eruptive deposits

Landslide

- Difficulties: small areas, localized and strong displacement, coherence loss but still possible

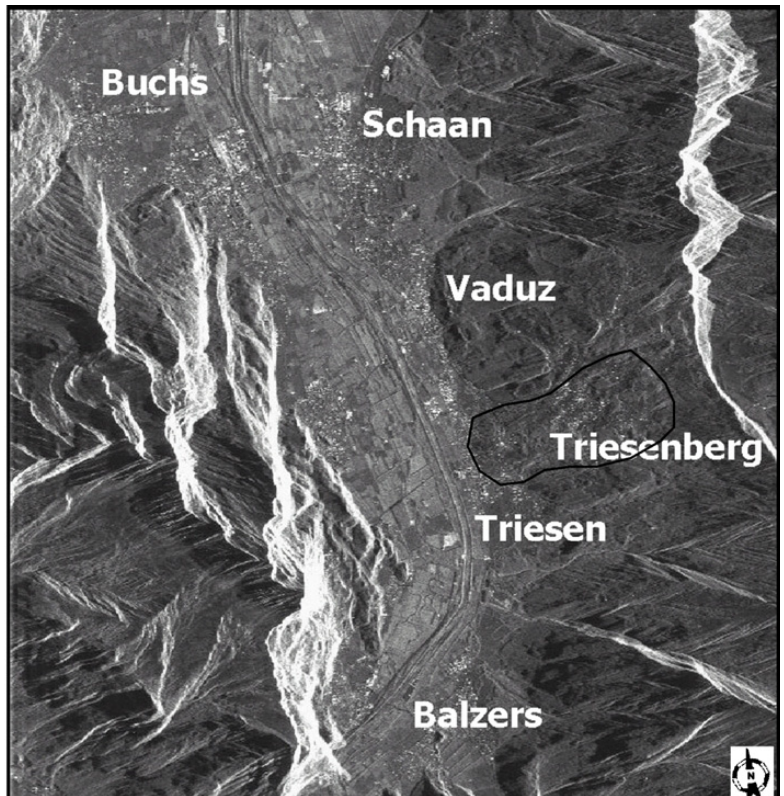

Cartography: Property of MapQuest - Web Site http://www.mapquest.com/atlas/main.adp

Colesanti, Wasowski, 2006

Landslide

- Difficulties: small areas, localized and strong displacement, coherence loss but still possible

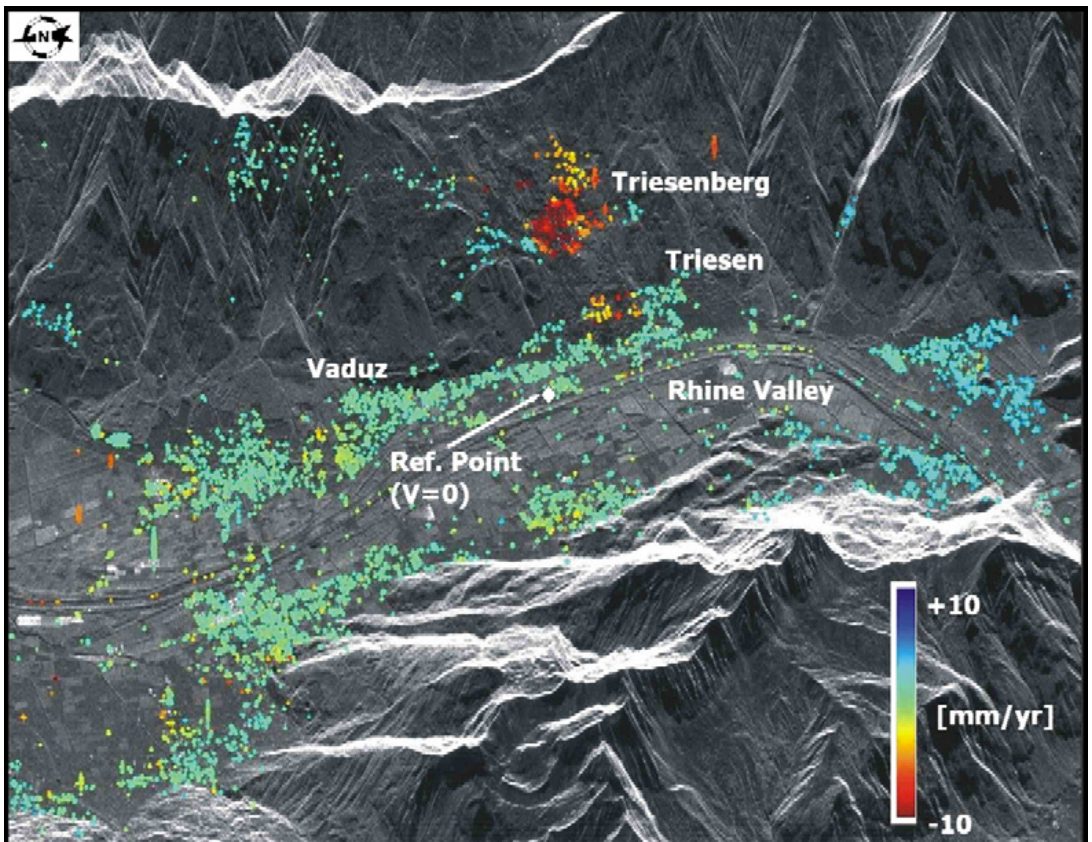

Colesanti, Wasowski, 2006

Landslide

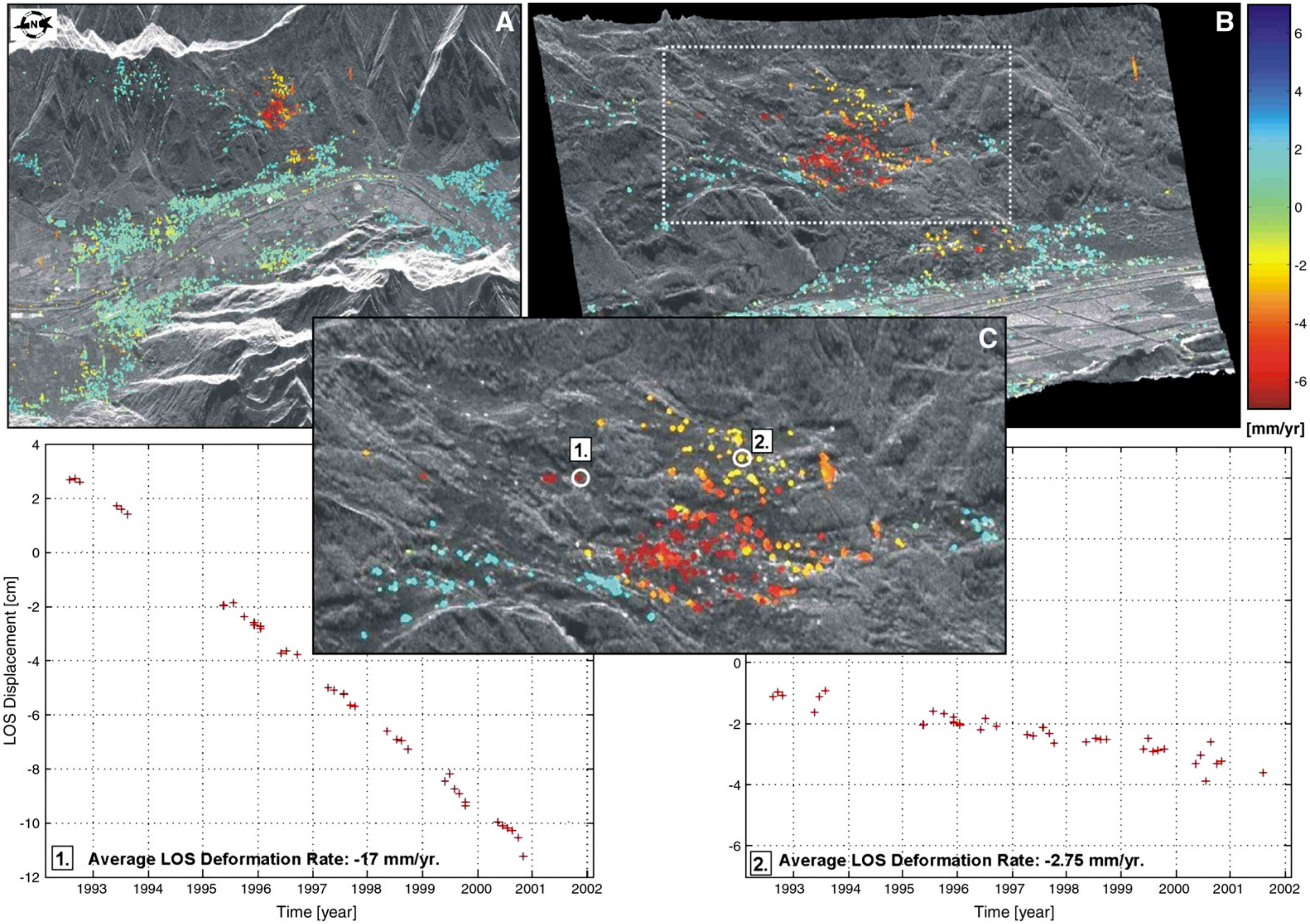

Colesanti, Wasowski, 2006

SAR application summary

- Production of surface displacement field maps:
  - Earthquakes (co-seismic)
  - Inter-seismic loading on faults
  - Landslides
  - Volcanoes
  - *Subsidence in urban areas*
- DEM production
- Detection of surface changes
  - Estimation of post-event damages
  - Mapping of eruptive deposits

Various type of volcanic deformation observed by INSAR

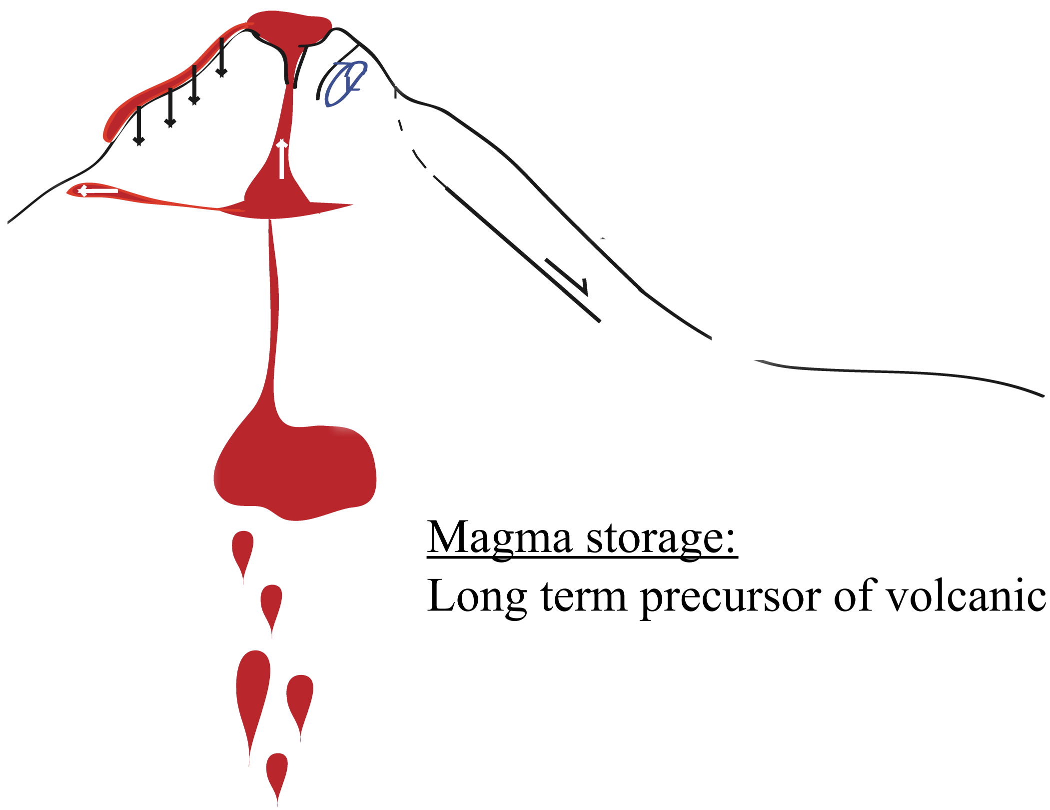

Magma storage:

Long term precursor of volcanic activity

InSAR performance

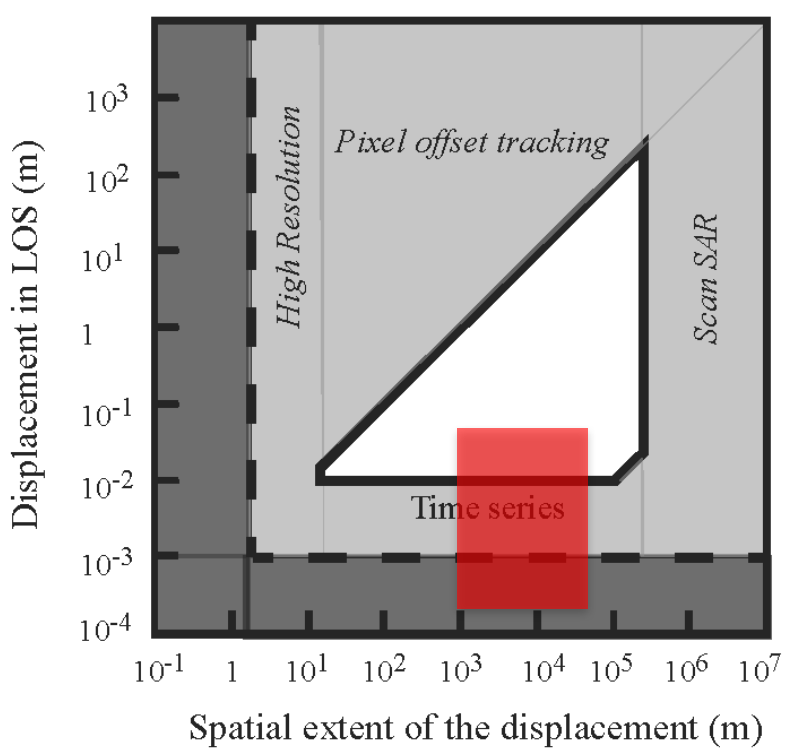

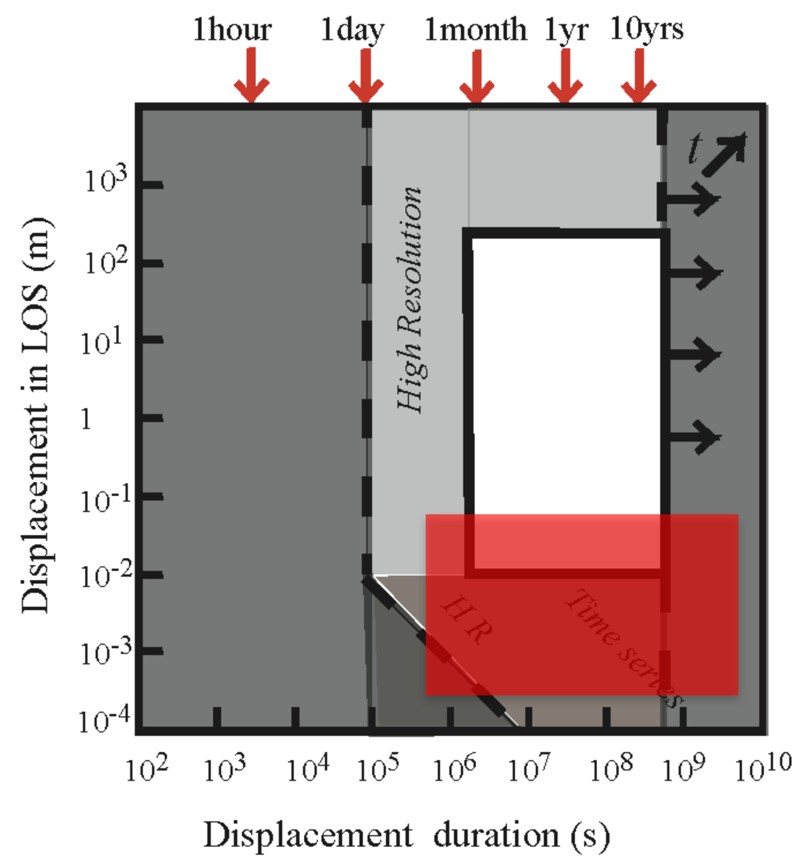

Magma storage

Various type of volcanic deformation observed by INSAR

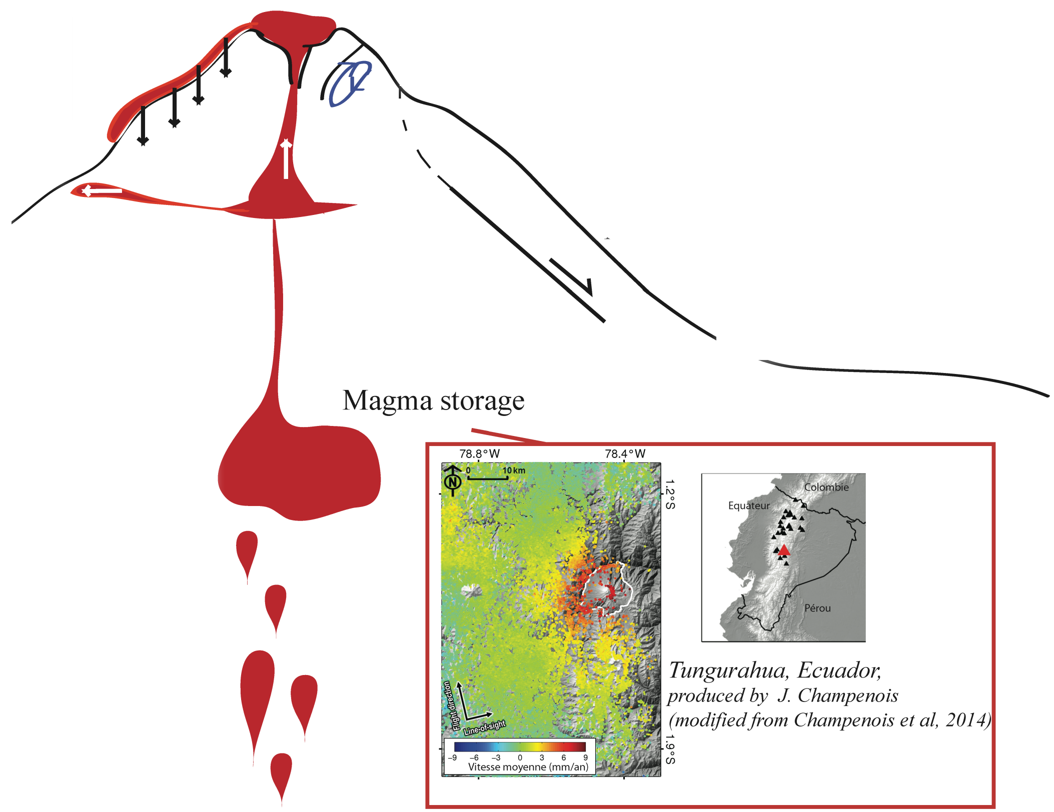

Various type of volcanic deformation observed by INSAR

Intrusions propagation:
Short term precursors of
Magmatic activity

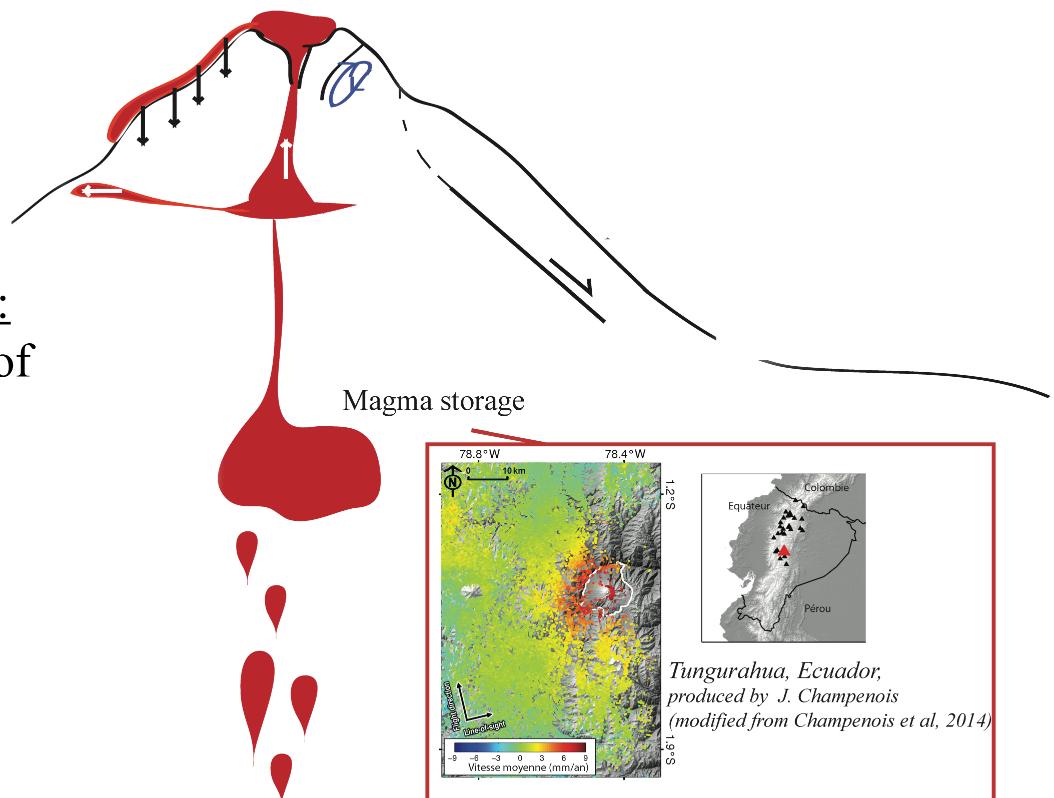

Tungurahua, Ecuador,
produced by J. Champenois
(modified from Champenois et al, 2014)

InSAR performance

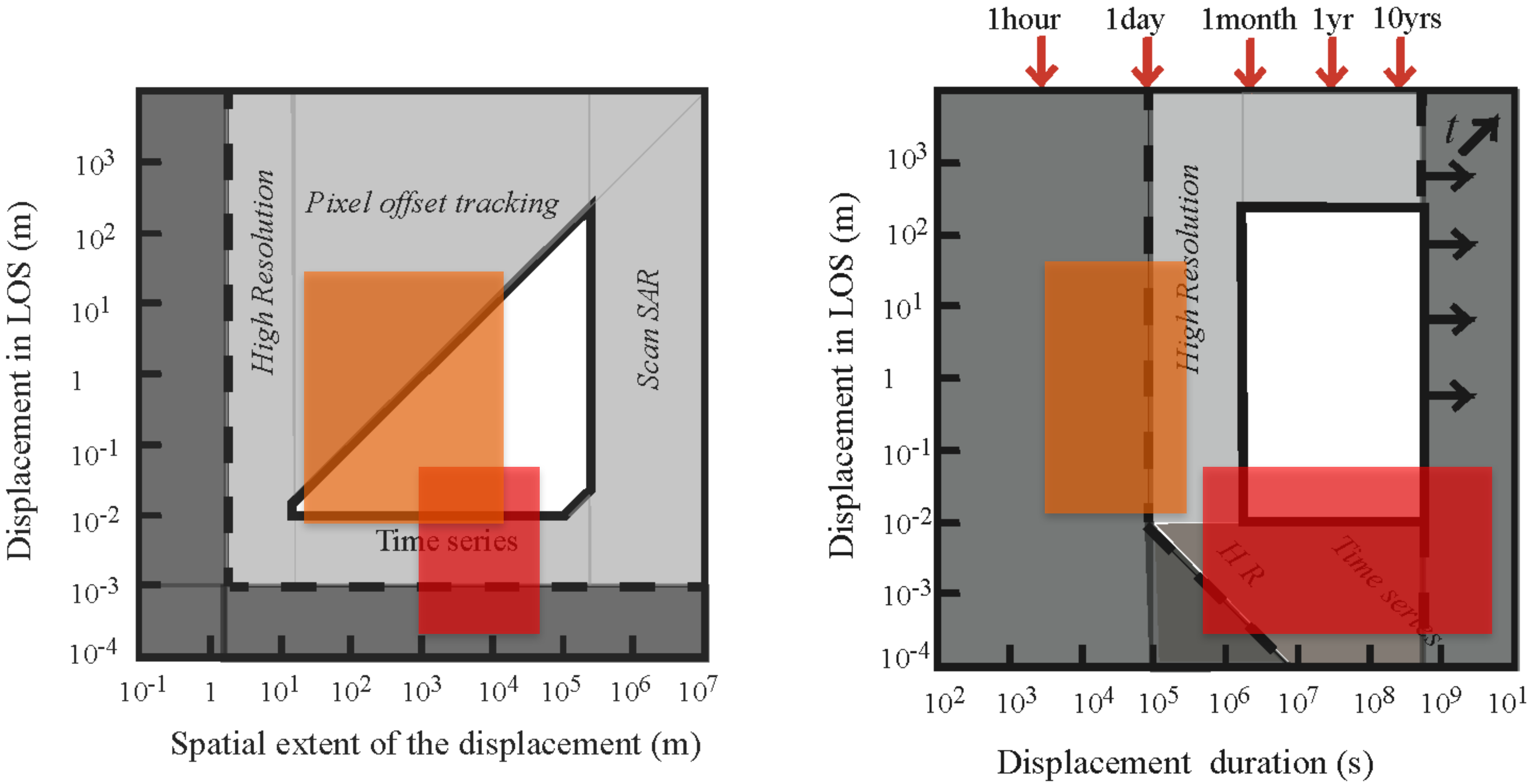

Magma storage

Dyke

Various type of volcanic deformation observed by INSAR

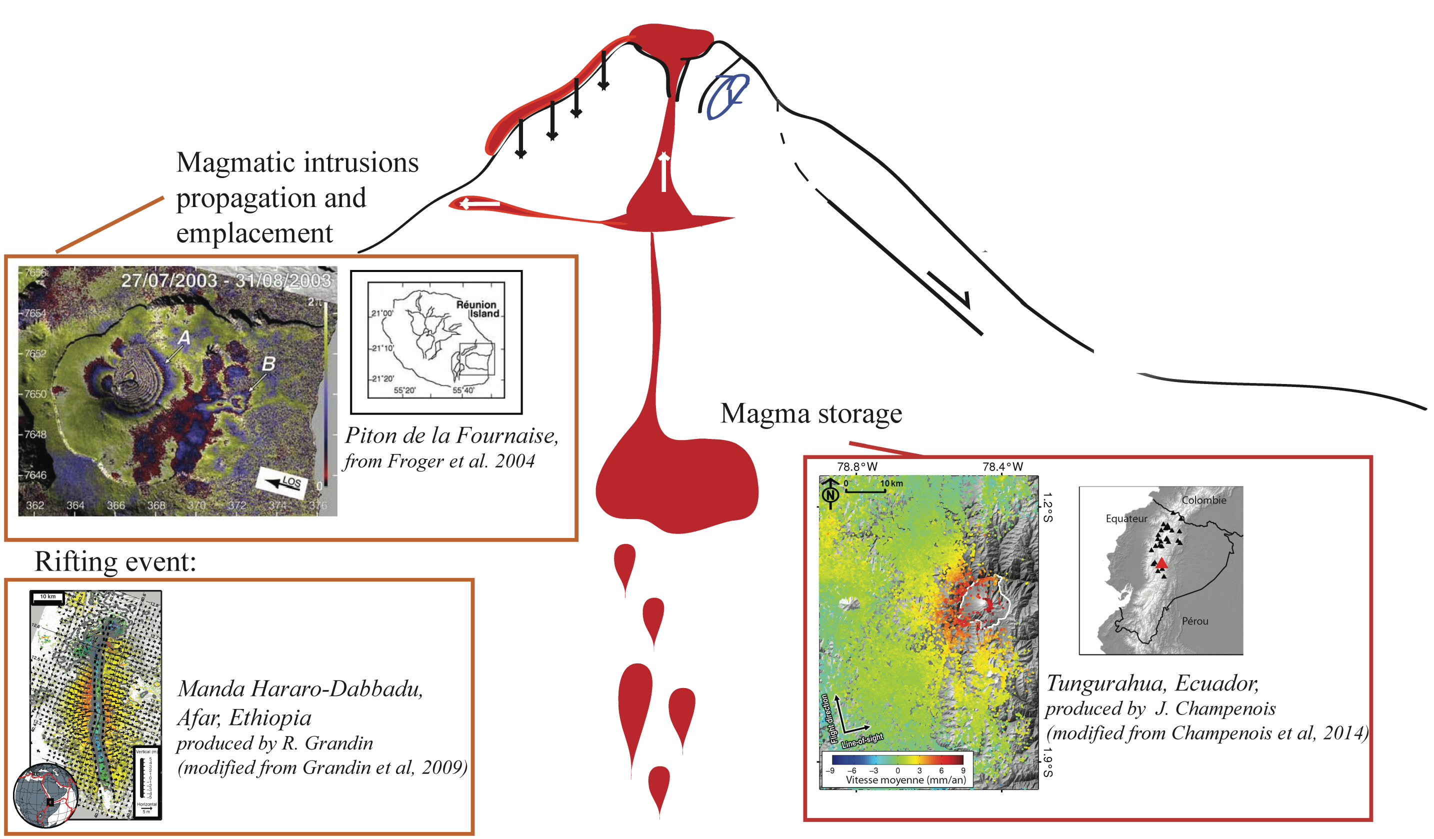

Various type of volcanic deformation observed by INSAR

<u>Magma flow in an open shallow conduit:</u>

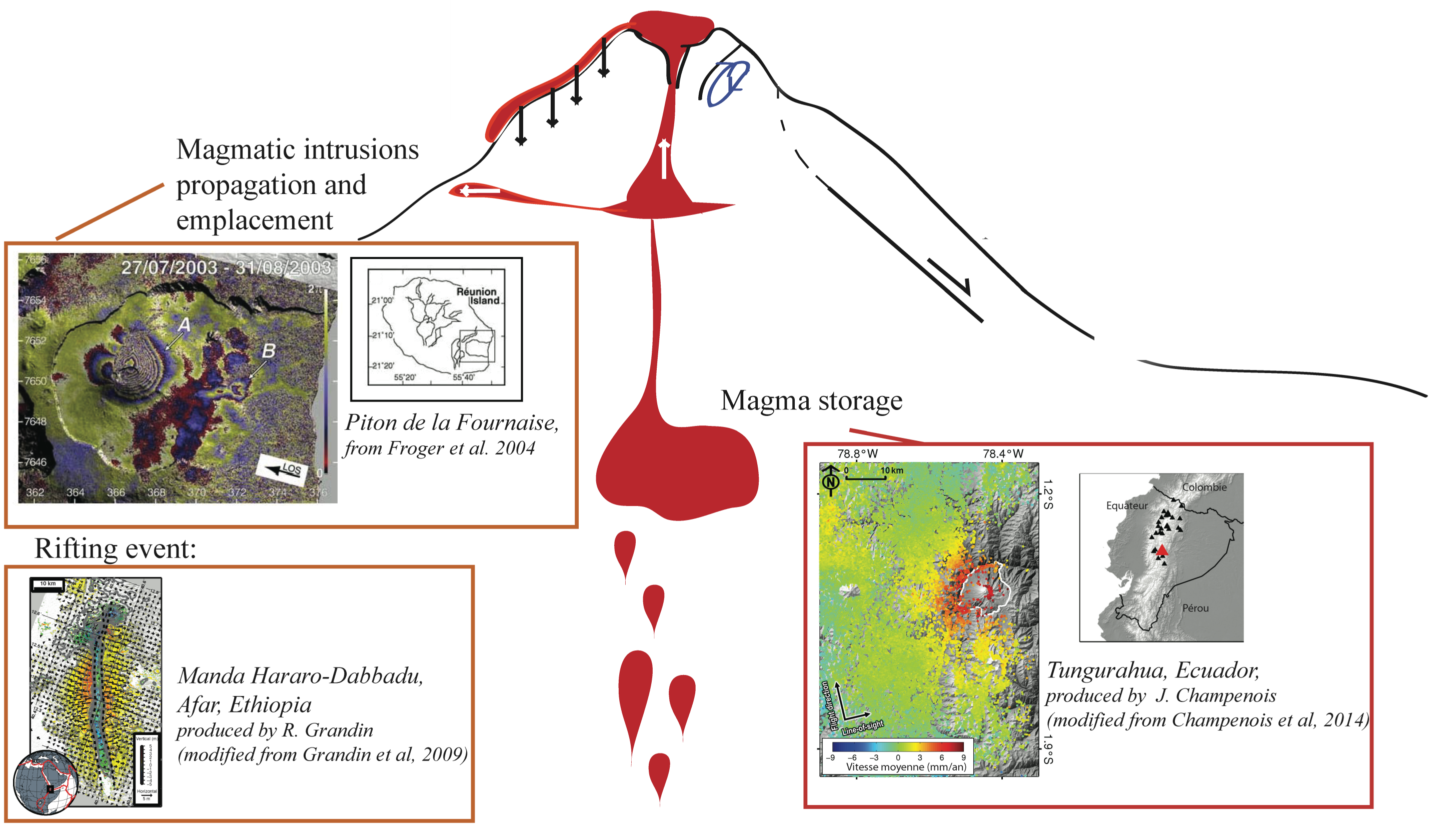

InSAR performance

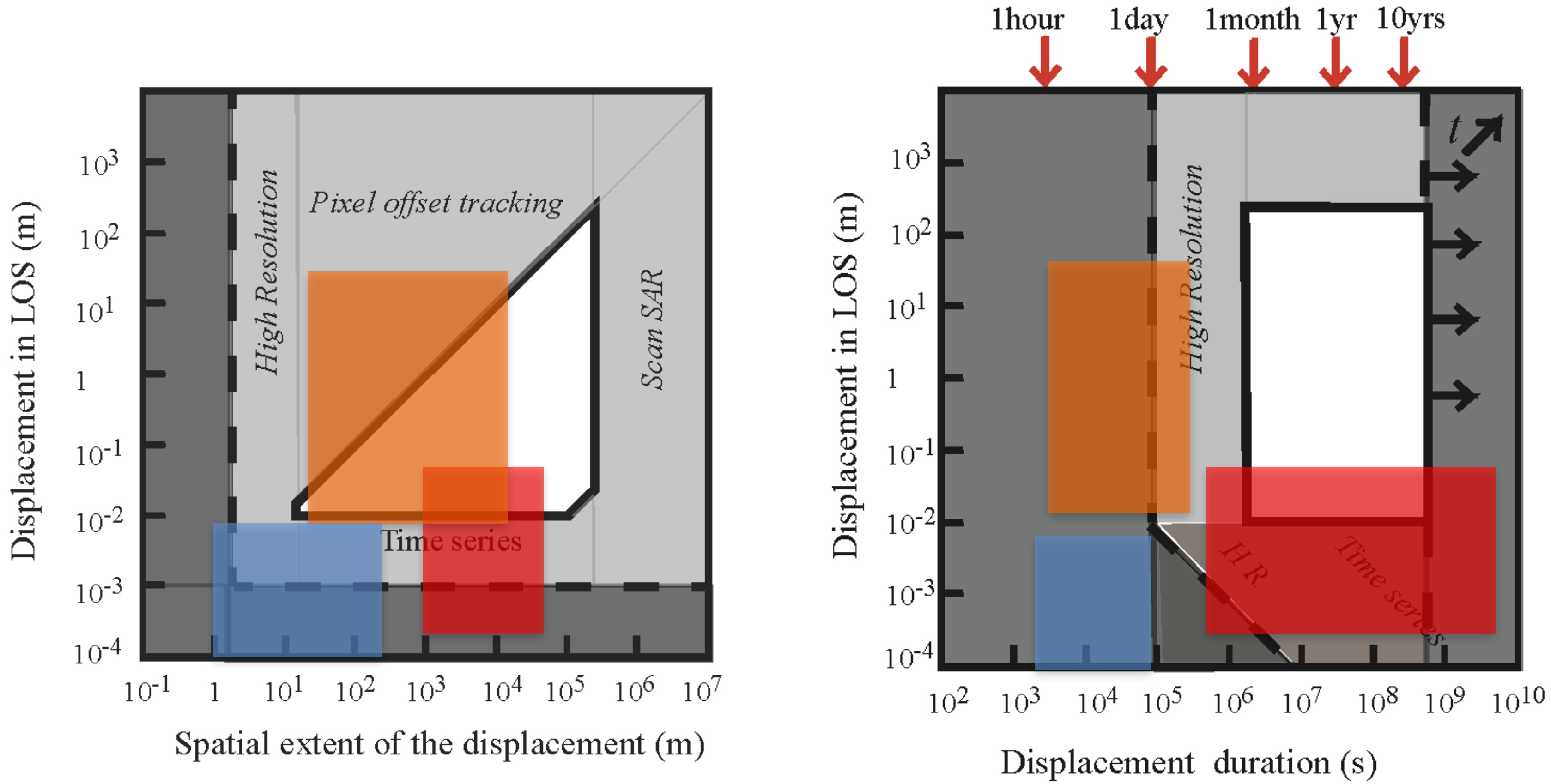

Magma storage

Conduit

Dyke

Various type of volcanic deformation observed by INSAR

Subsidence on eruptive deposits:

Magmatic intrusions propagation and emplacement

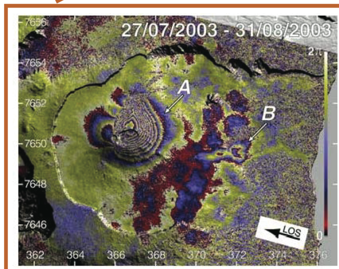

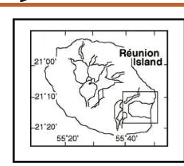

Piton de la Fournaise, from Froger et al. 2004

Rifting event:

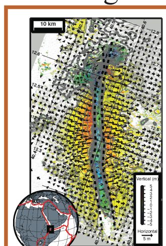

Manda Hararo-Dabbadu, Afar, Ethiopia
produced by R. Grandin
(modified from Grandin et al, 2009)

Magma storage

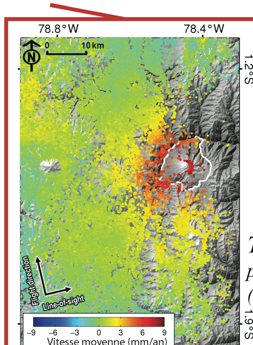

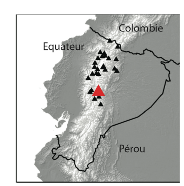

Tungurahua, Ecuador,
produced by J. Champenois
(modified from Champenois et al, 2014)

InSAR performance

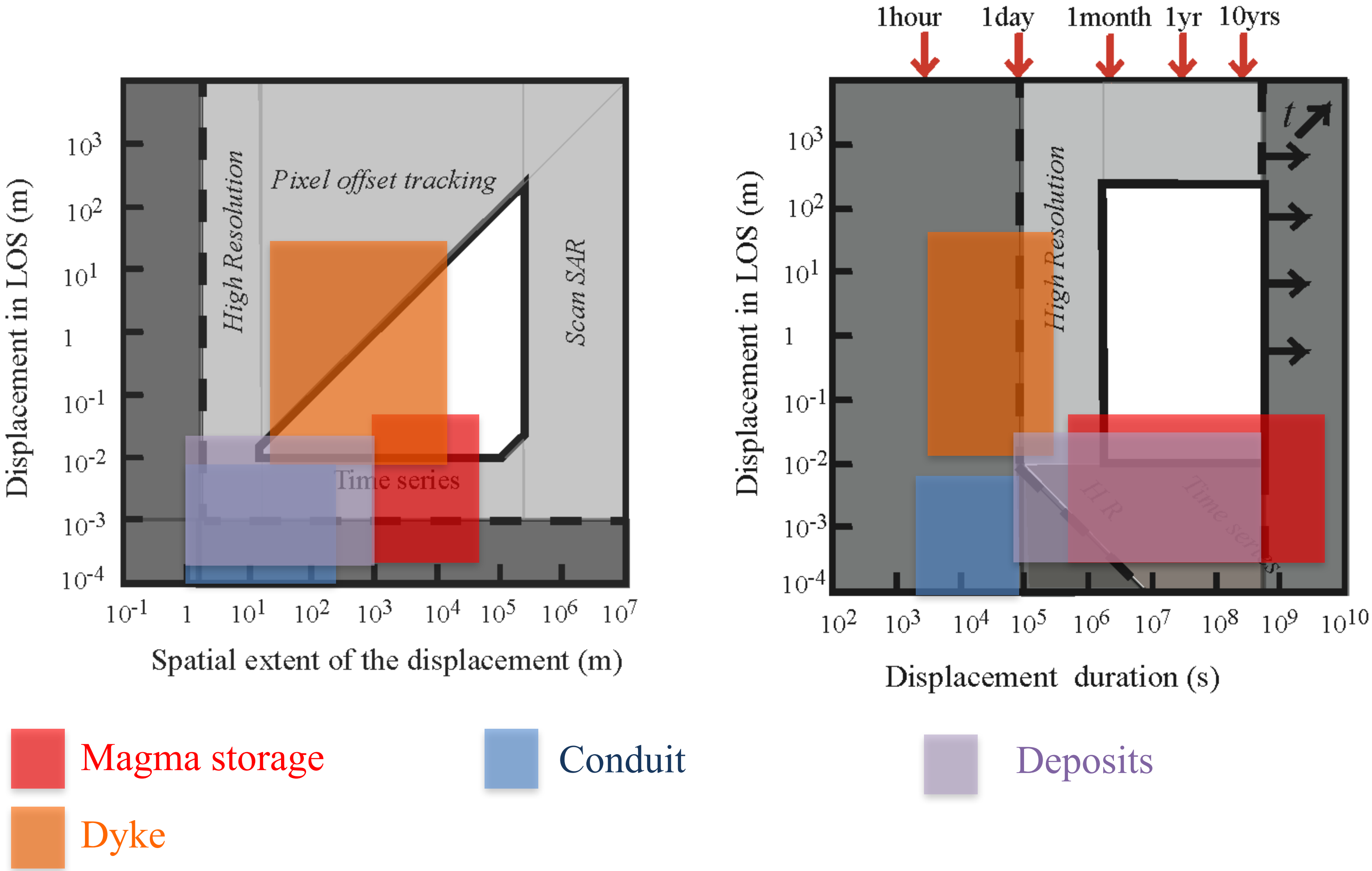

Various type of volcanic deformation observed by INSAR

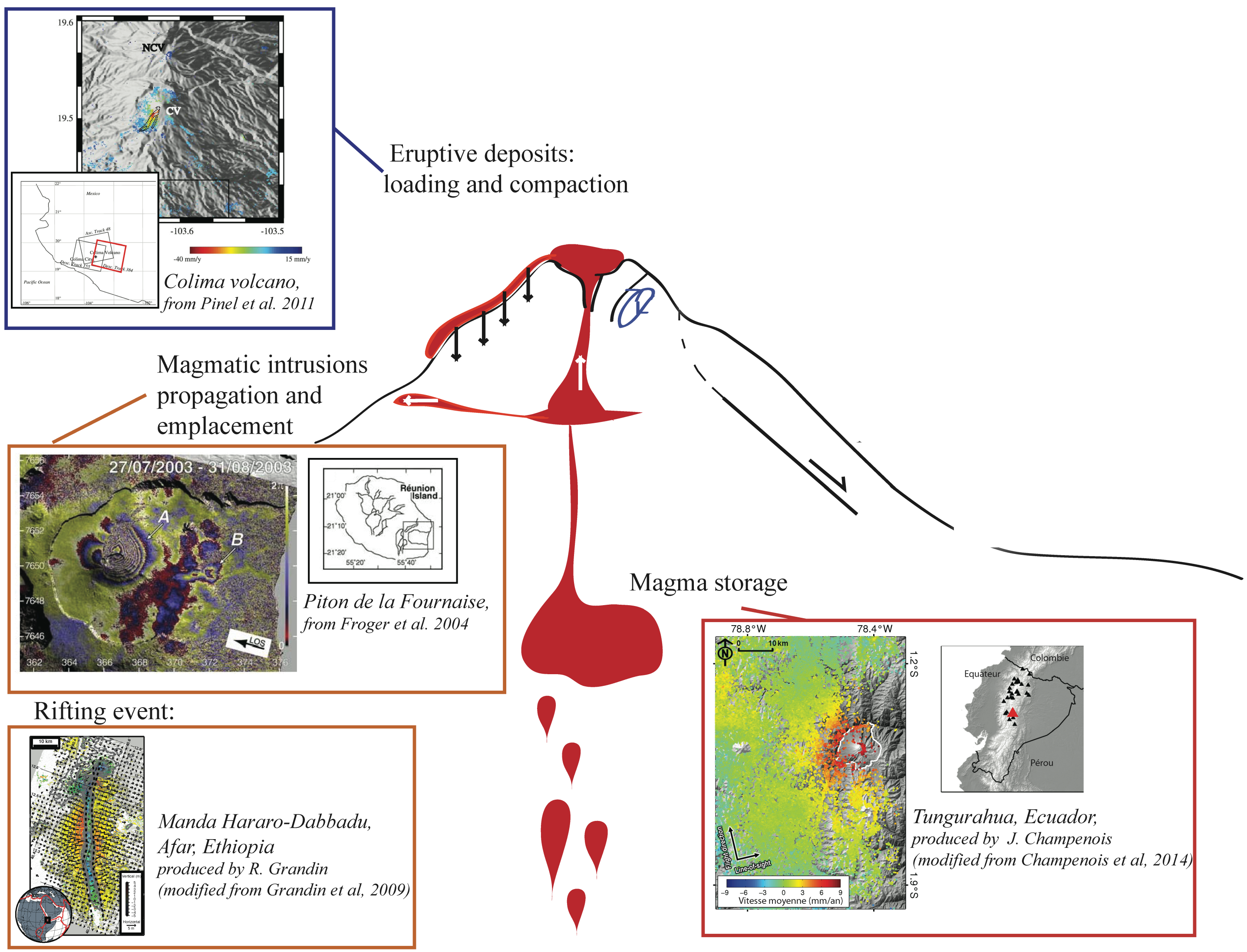

Various type of volcanic deformation observed by INSAR

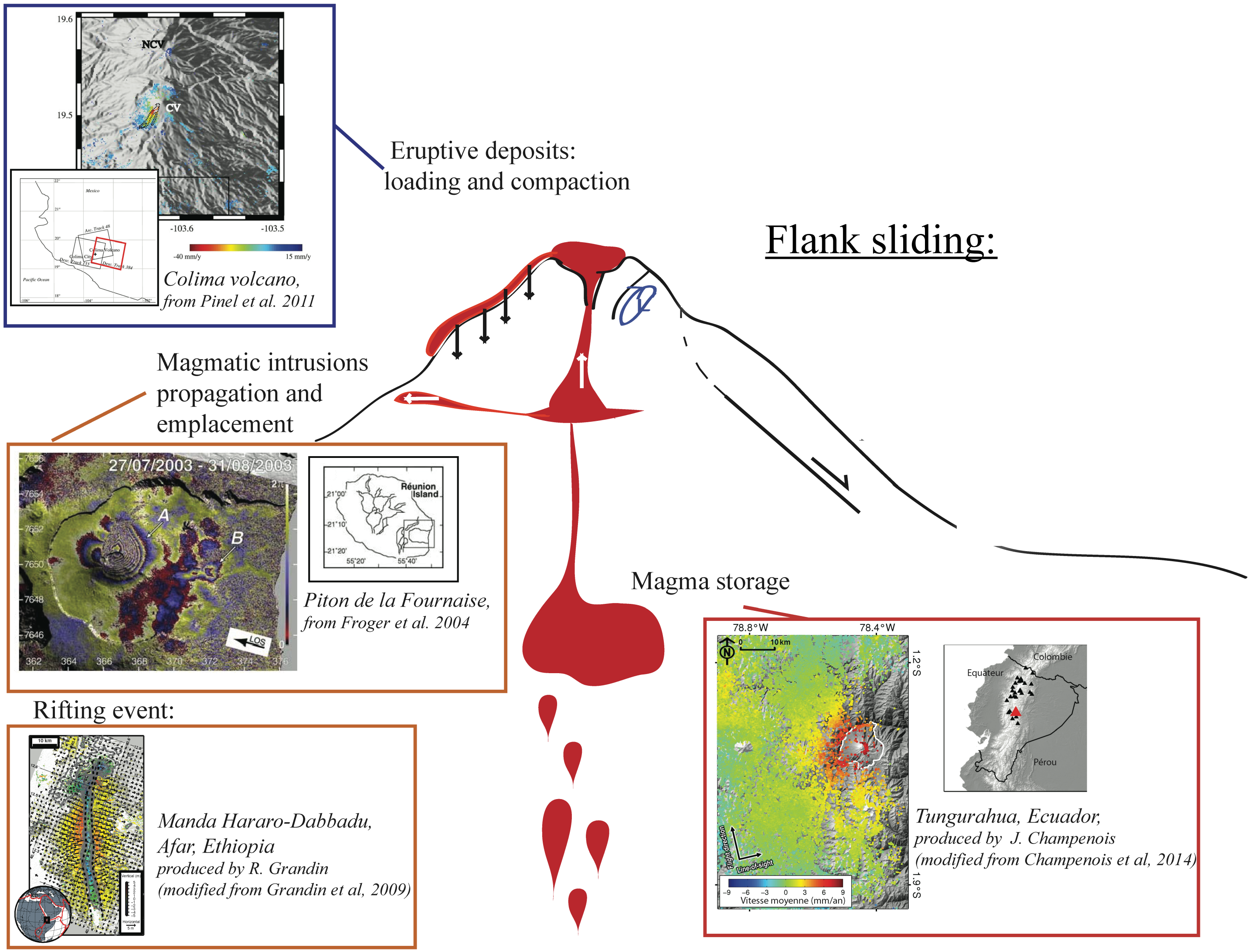

InSAR performance

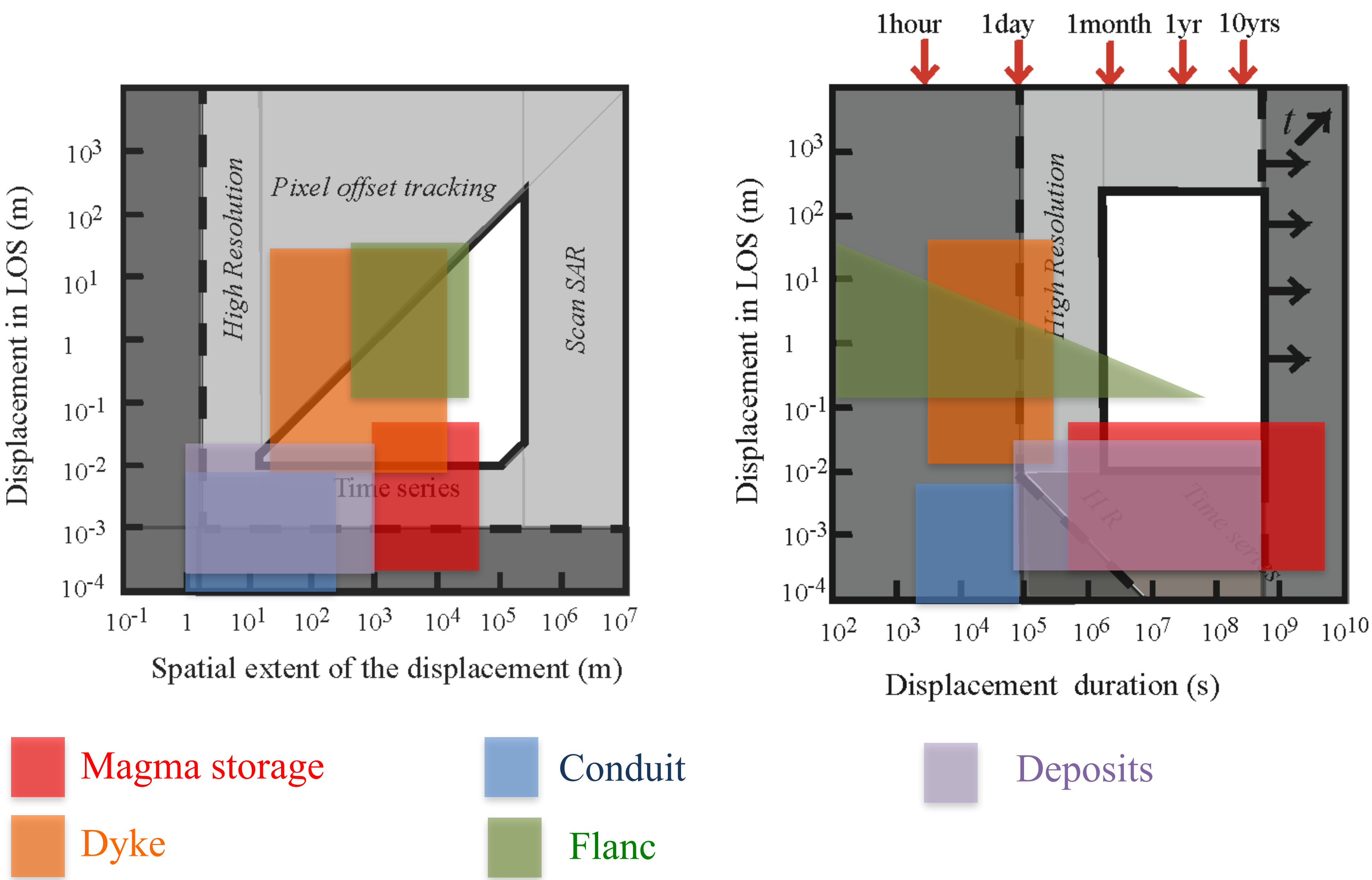

Various type of volcanic deformation observed by INSAR

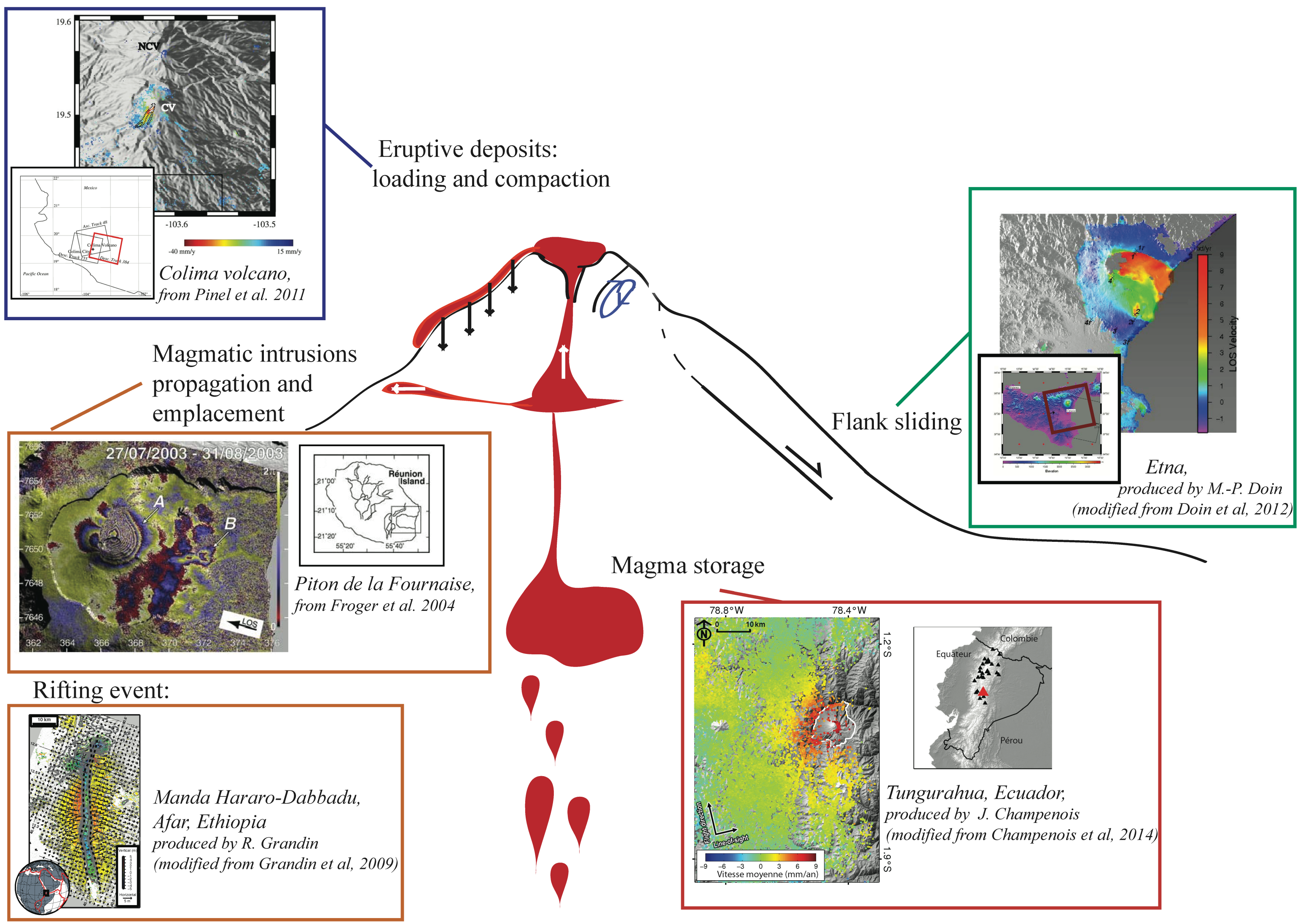

Various type of volcanic deformation observed by INSAR

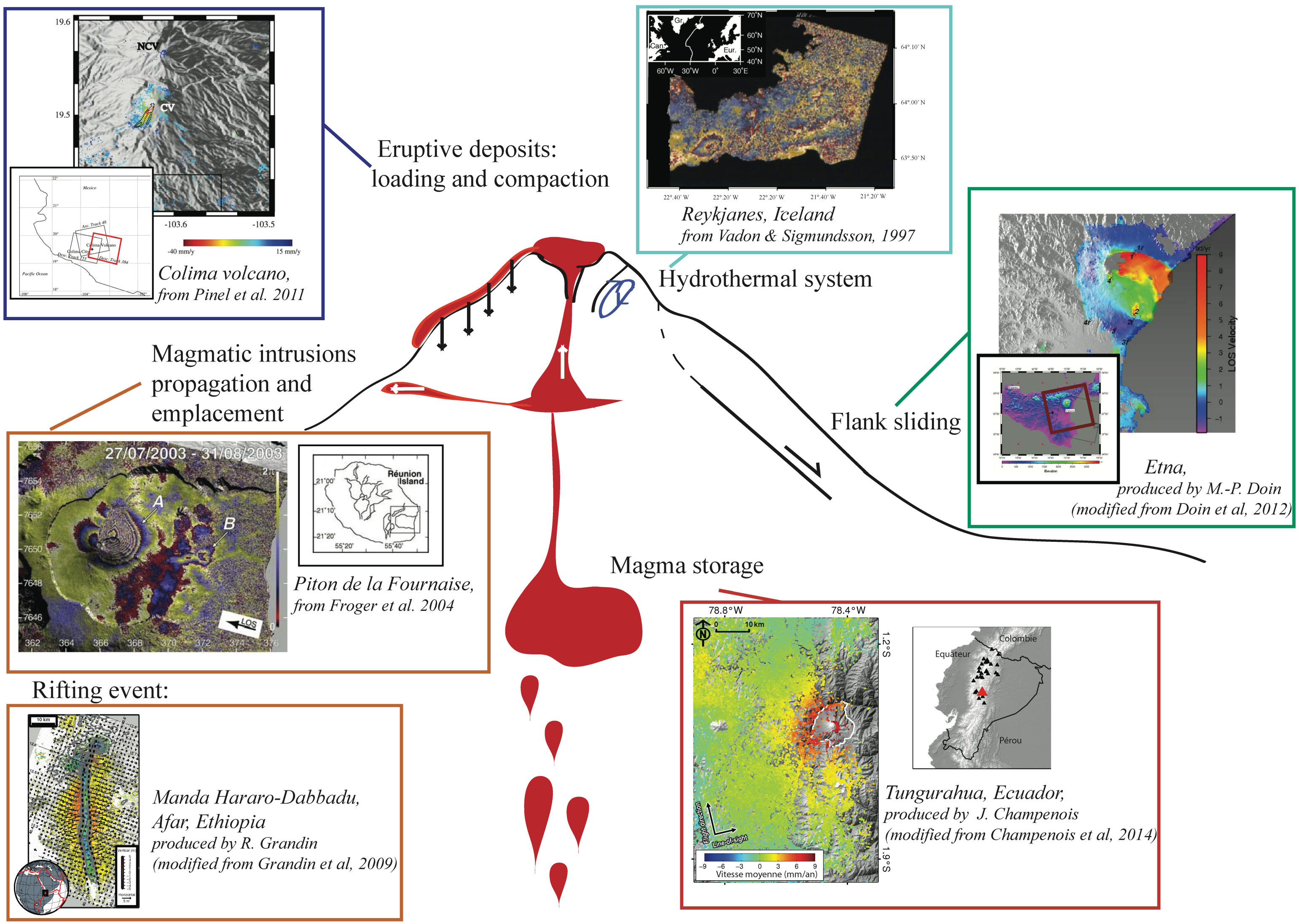

Exceptional events have been imaged

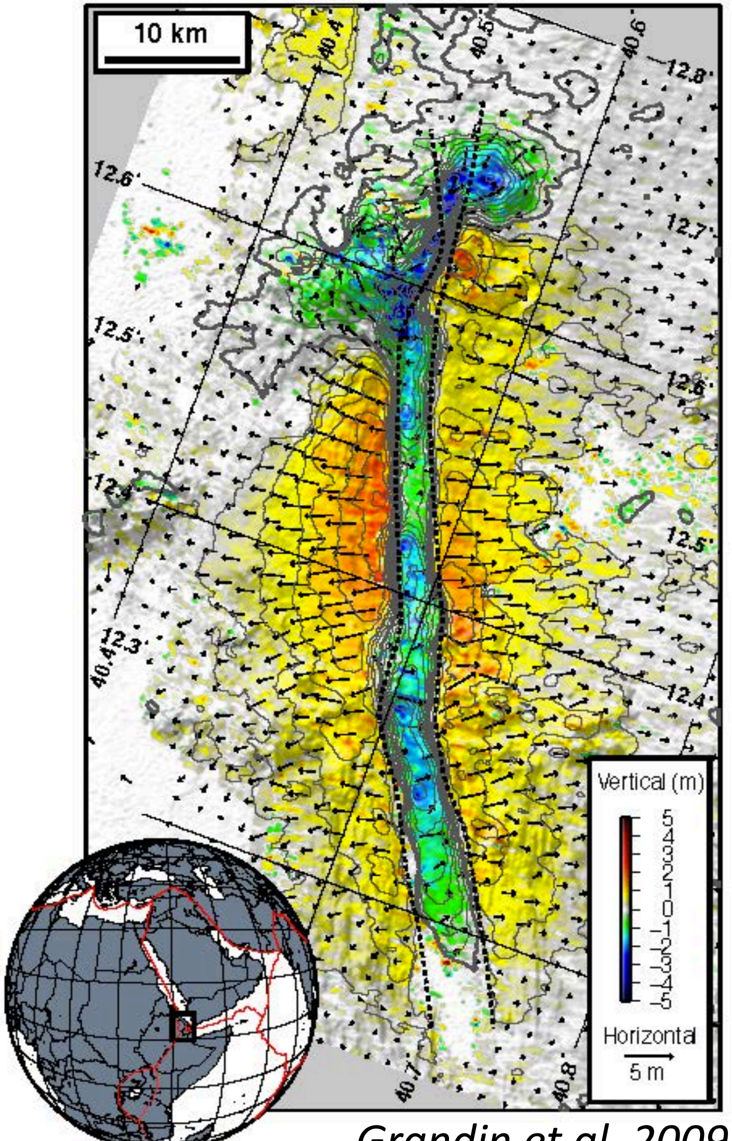

Grandin et al, 2009

Wright et al,Nature, 2006

Exceptional events have been imaged

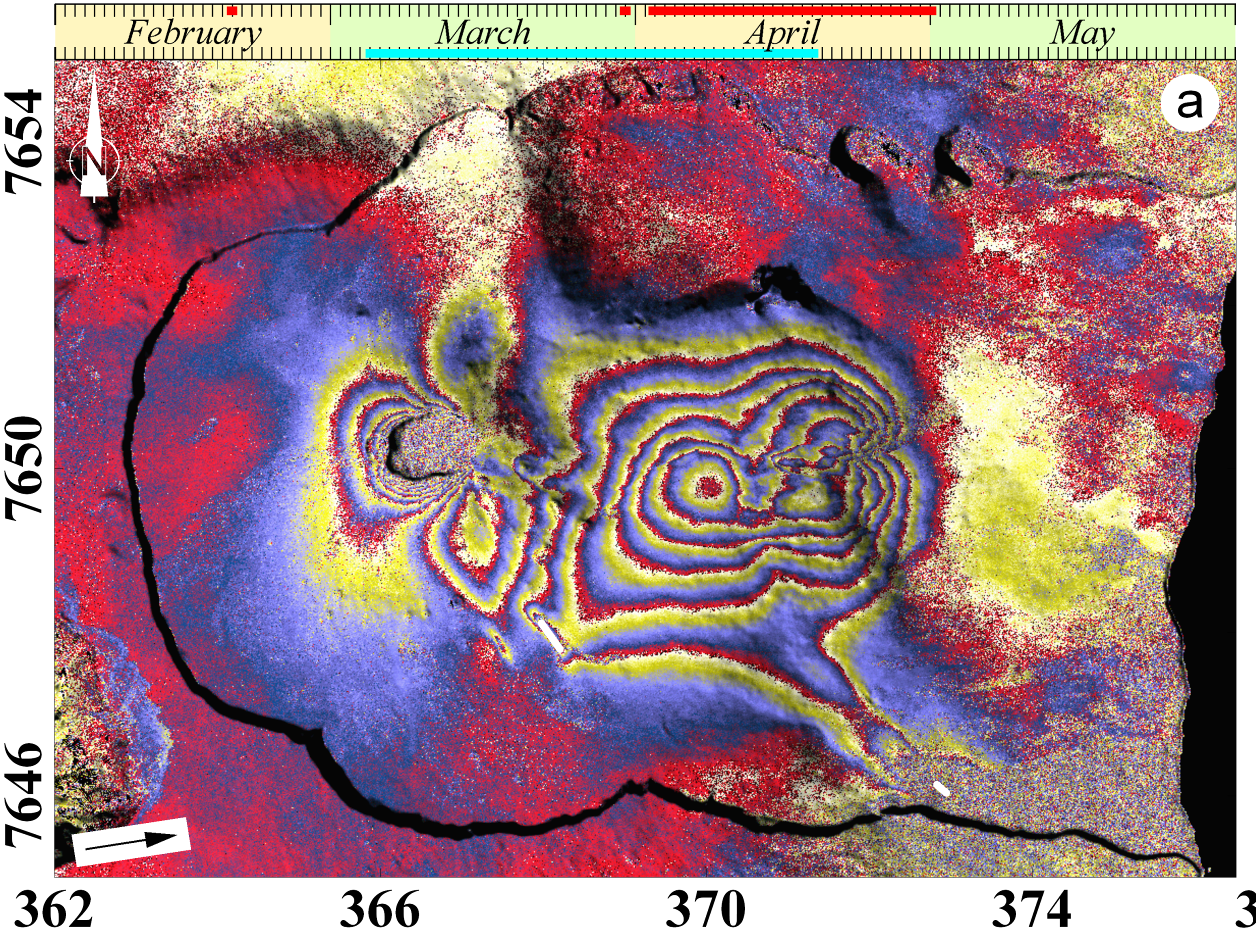

Froger et al., 2015

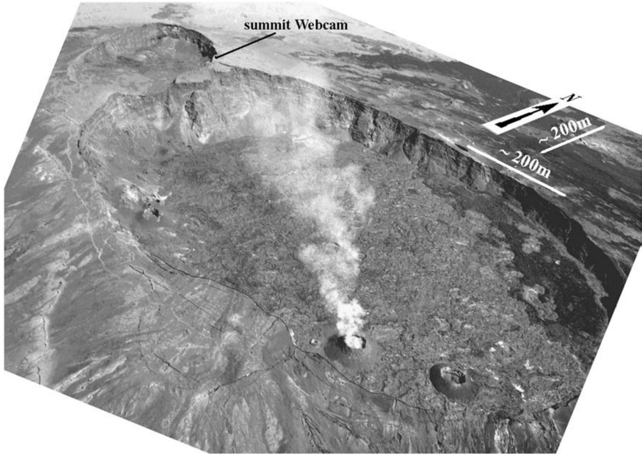

Staudacher et al., 2009

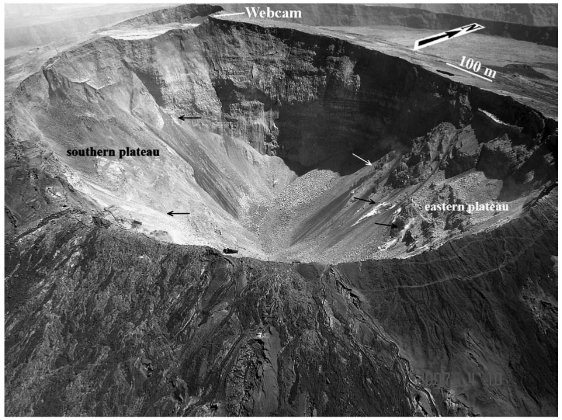

Deformation observed on more than 160 volcanoes and statistics

Biggs et al, Nat. Com., 2014

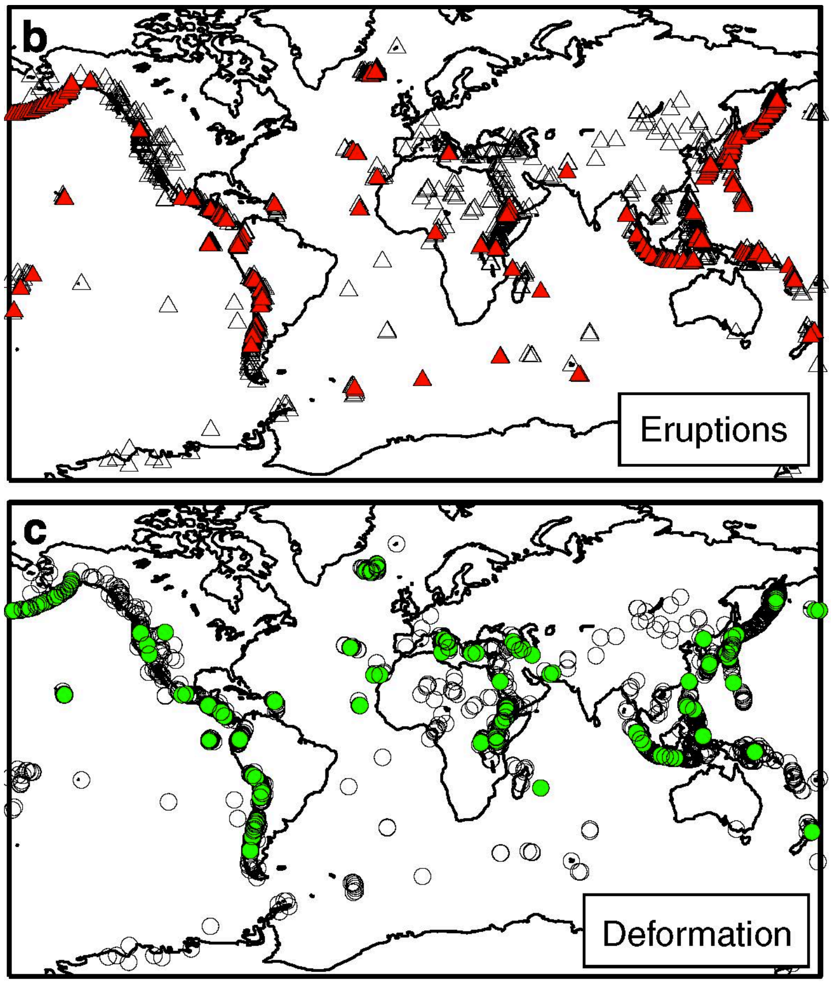

Systematic Coverage $N=540$ $P=0.13$	Erupted	Non-Erupted
Deformed	DE 25 True positive	$D\bar{E}$ 29 False positive
Non-deformed	$\bar{D}E$ 9 False negative	$\bar{D}\bar{E}$ 135 True negative

Deformation observed on more than 160 volcanoes and statistics

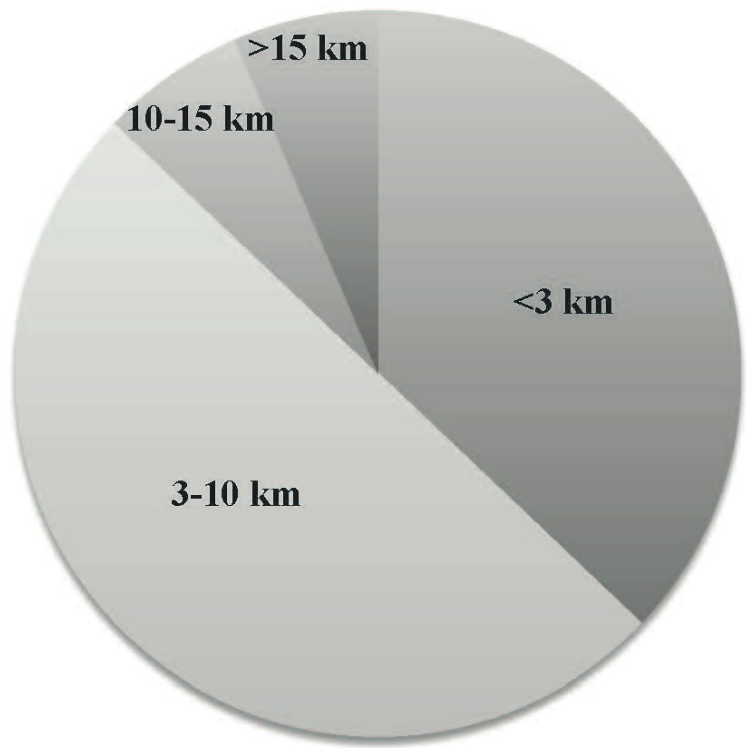

Profondeur des zones de stockage

Pinel et al, 2014

Deformation/volcanic activity in the Andes as revealed by InSAR

Eruption
No deformation detected by InSAR

Nevado del Huila Colombia
Guagua Pichincha, Ecuador
Ubinas, Peru
Irruputuncu, Chile
Planchon Peteroa, Chile
Villarica, Chile

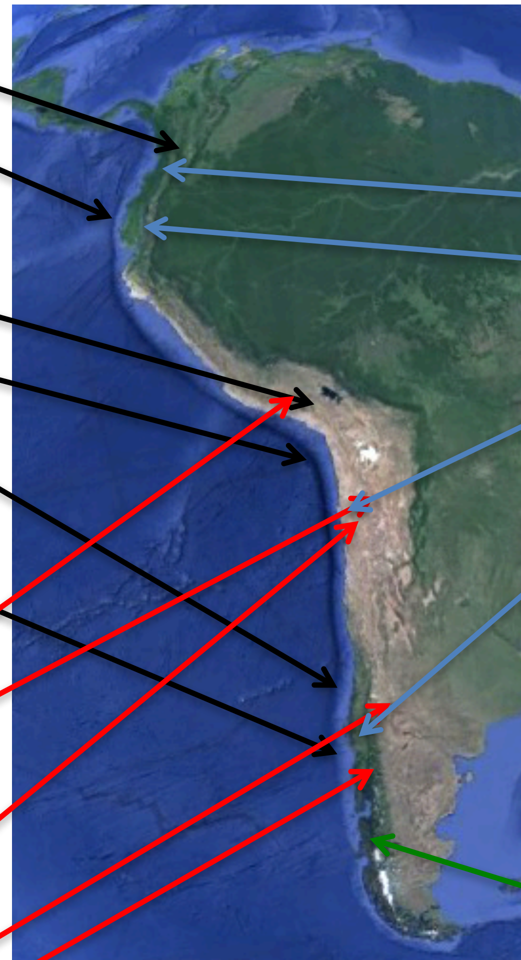

Eruption
Co or post-eruptive deformation

Galeras, Colombia
Tungurahua, Ecuador
Lascar, Chile
Llaima, Chile

No eruption
Long-term inflation

Hualca Hualca, Peru
Uturuncu, Bolivia
Lazufre, Chile-Argentina
Laguna del Maule, Chile
Cordon Caulle, Chile

Eruption
Pre-eruptive inflation

Cerro Hudson, Chile

From Biggs et al, 2014

Deformation/volcanic activity in the Andes as revealed by InSAR

Eruption
No deform

Nevado de

Guagua Pi

Ubinas, Pe

Irruputunc

Planchon I

Villarica, C

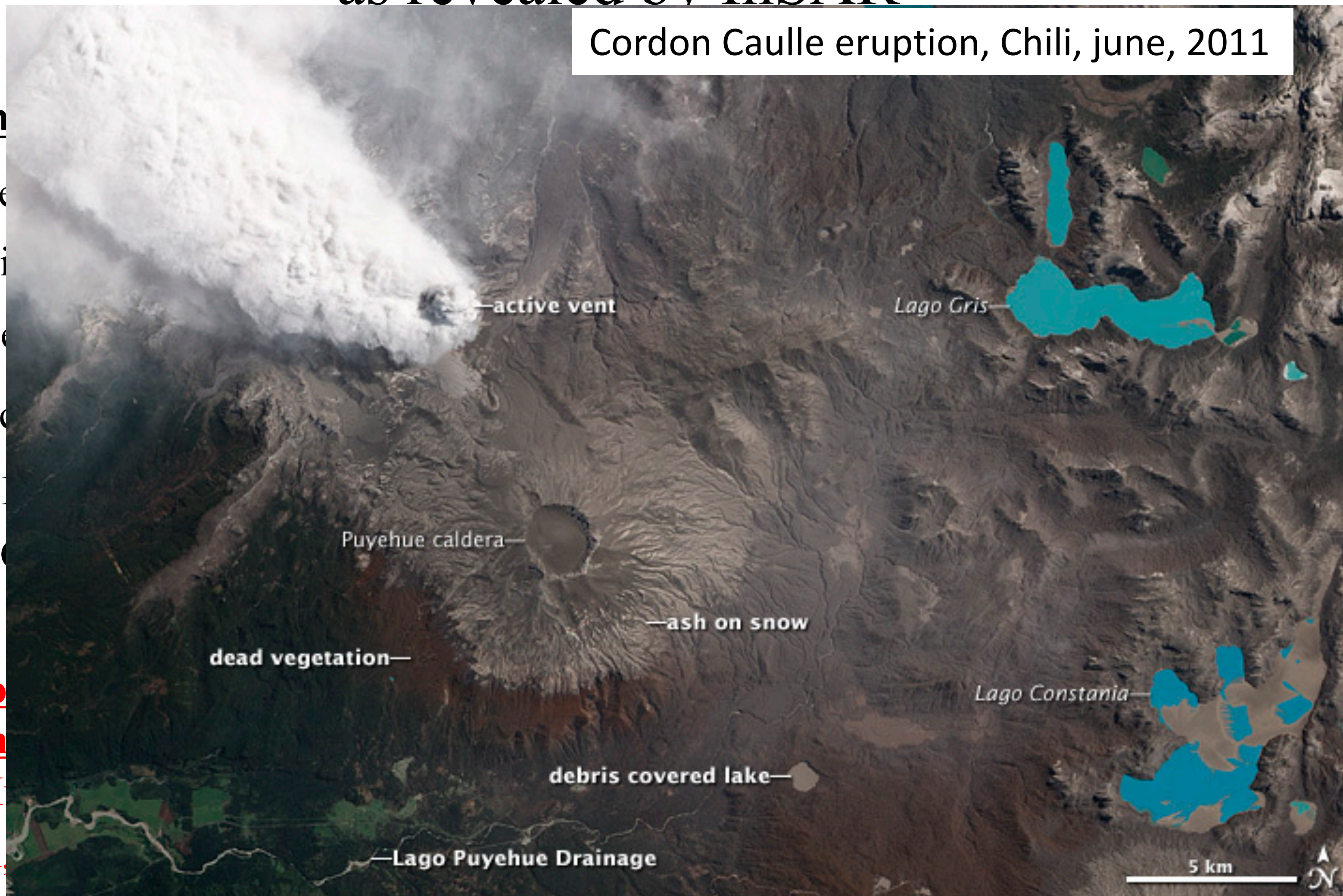

ation

dor

No eruptio
Long-term

Hualca H

Uturuncu,

Lazufre, Chile-Argentina

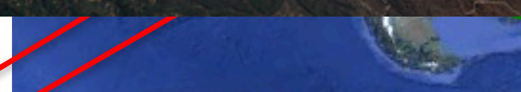

Cerro Hudson, Chile

Laguna del Maule, Chile
Cordon Caulle, Chile

From Biggs et al, 2014

Deformation/volcanic activity in the Andes as revealed by InSAR

Eruption
No deformation detected by InSAR

Nevado del Huila Colombia
Guagua Pichincha, Ecuador
Ubinas, Peru
Irruputuncu, Chile
Planchon Peteroa, Chile
Villarica, Chile

Eruption
Co or post-eruptive deformation

Galeras, Colombia
Tungurahua, Ecuador
Lascar, Chile
Llaima, Chile

No eruption
Long-term inflation

Hualca Hualca, Peru
Uturuncu, Bolivia
Lazufre, Chile-Argentina
Laguna del Maule, Chile

Eruption
Pre-eruptive inflation

Cordon Caulle, Chile
Cerro Hudson, Chile

From Biggs et al, 2014

Deformation/volcanic activity in the Andes as revealed by InSAR

Eruption
No deformation detected by InSAR

- Nevado del Huila Colombia
- Guagua Pichincha, Ecuador
- Ubinas, Peru
- Irruputuncu, Chile
- Planchon Peteroa, Chile
- Villarica, Chile

Eruption
Co or post-eruptive deformation

- Galeras, Colombia
- Tungurahua, Ecuador
- Lascar, Chile
- Llaima, Chile

No eruption
Long-term inflation

- Hualca Hualca, Peru
- Uturuncu, Bolivia
- Lazufre, Chile-Argentina
- Laguna del Maule, Chile

Eruption
Pre-eruptive inflation

- Cordon Caulle, Chile
- Cerro Hudson, Chile

From Biggs et al, 2014

Tungurahua, Ecuador

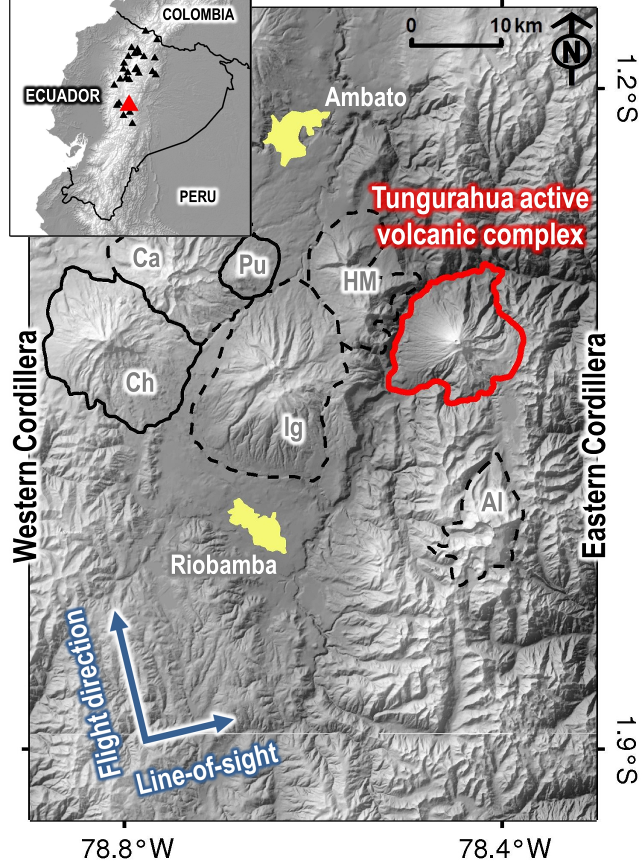

Eruptive rate of 1.5 million m^3/yr over the last 2300 yr
(Hall et al., 99)

Data set and processing method

* 22 ENVISAT images (C-band, ascending track 447, incidence angle=23°)

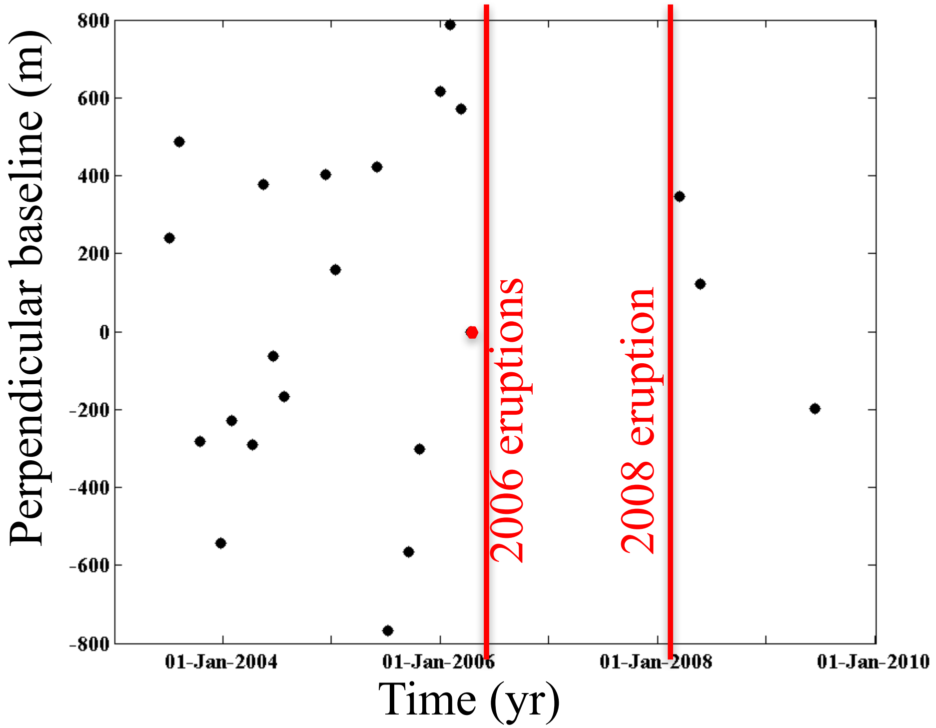

* StaMPS (Hooper et al, 2004) using the SRTM DEM

Time series of LOS displacement

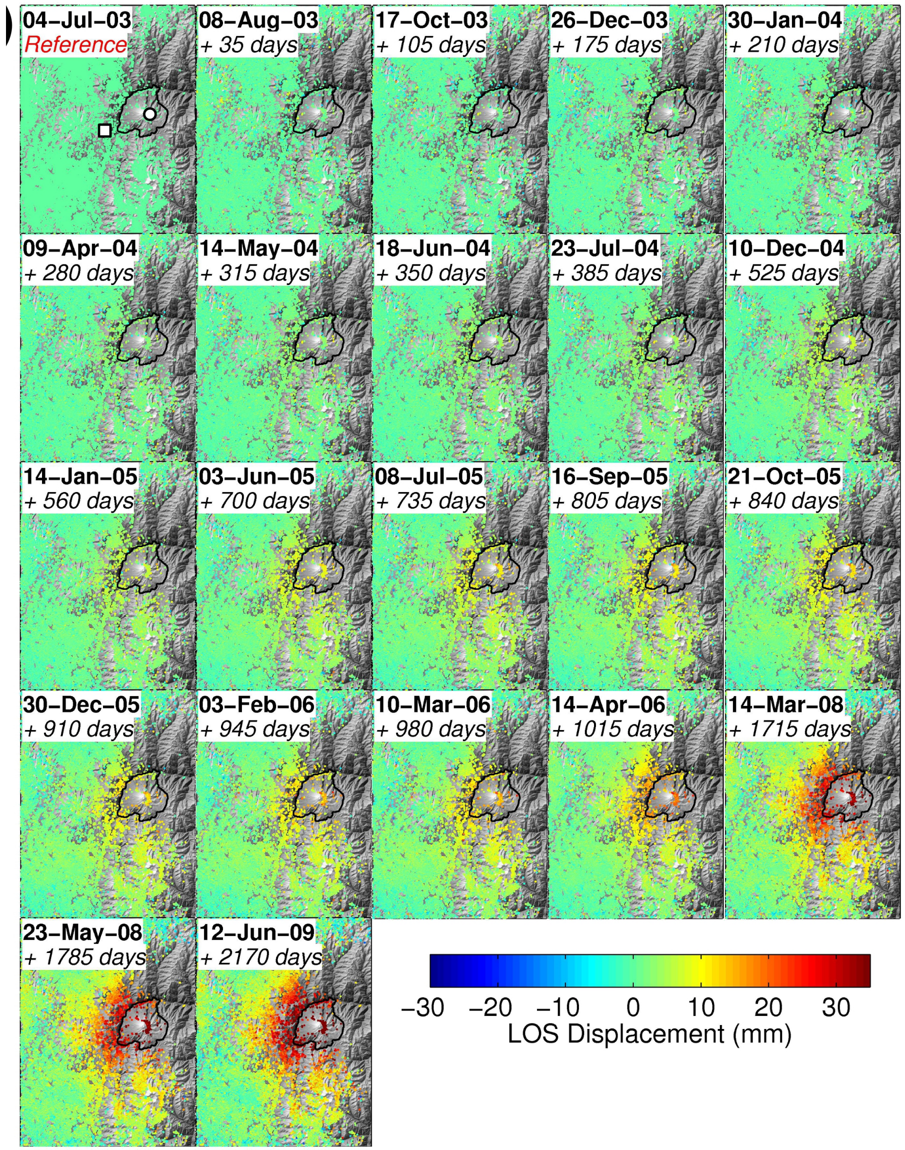

Large scale uplift (25km in radius)

Mean velocity

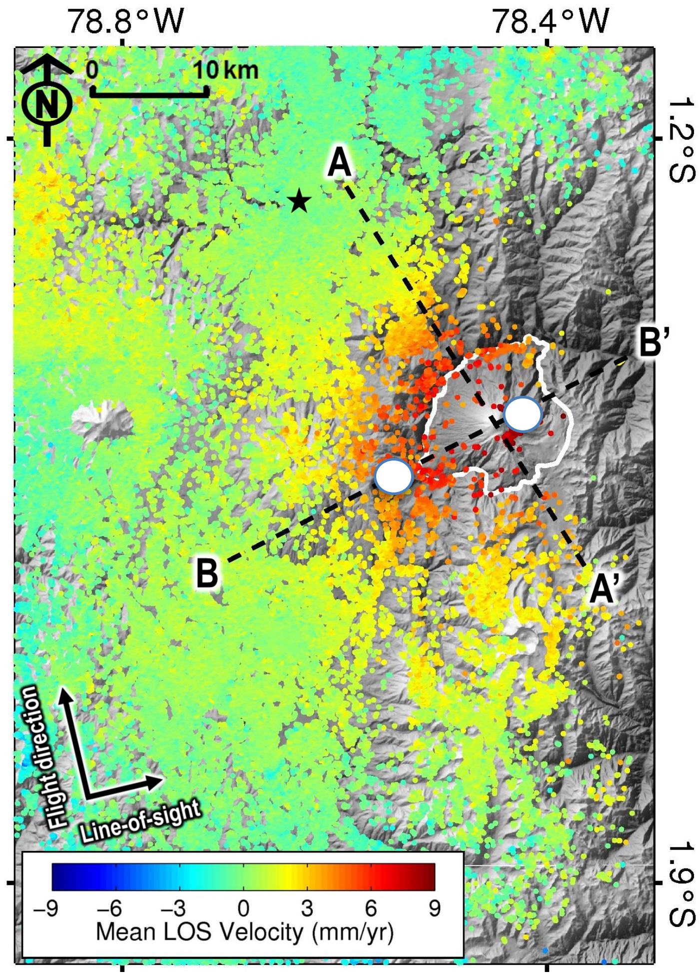

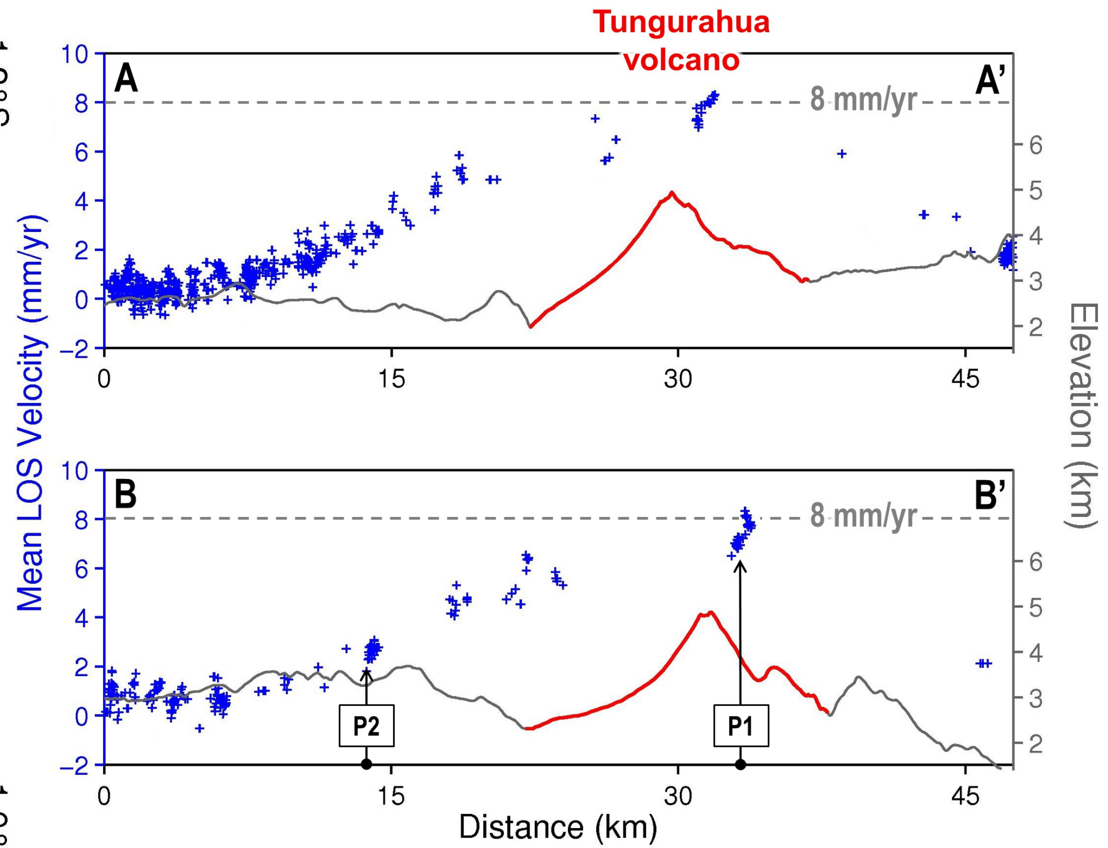

Temporal evolution

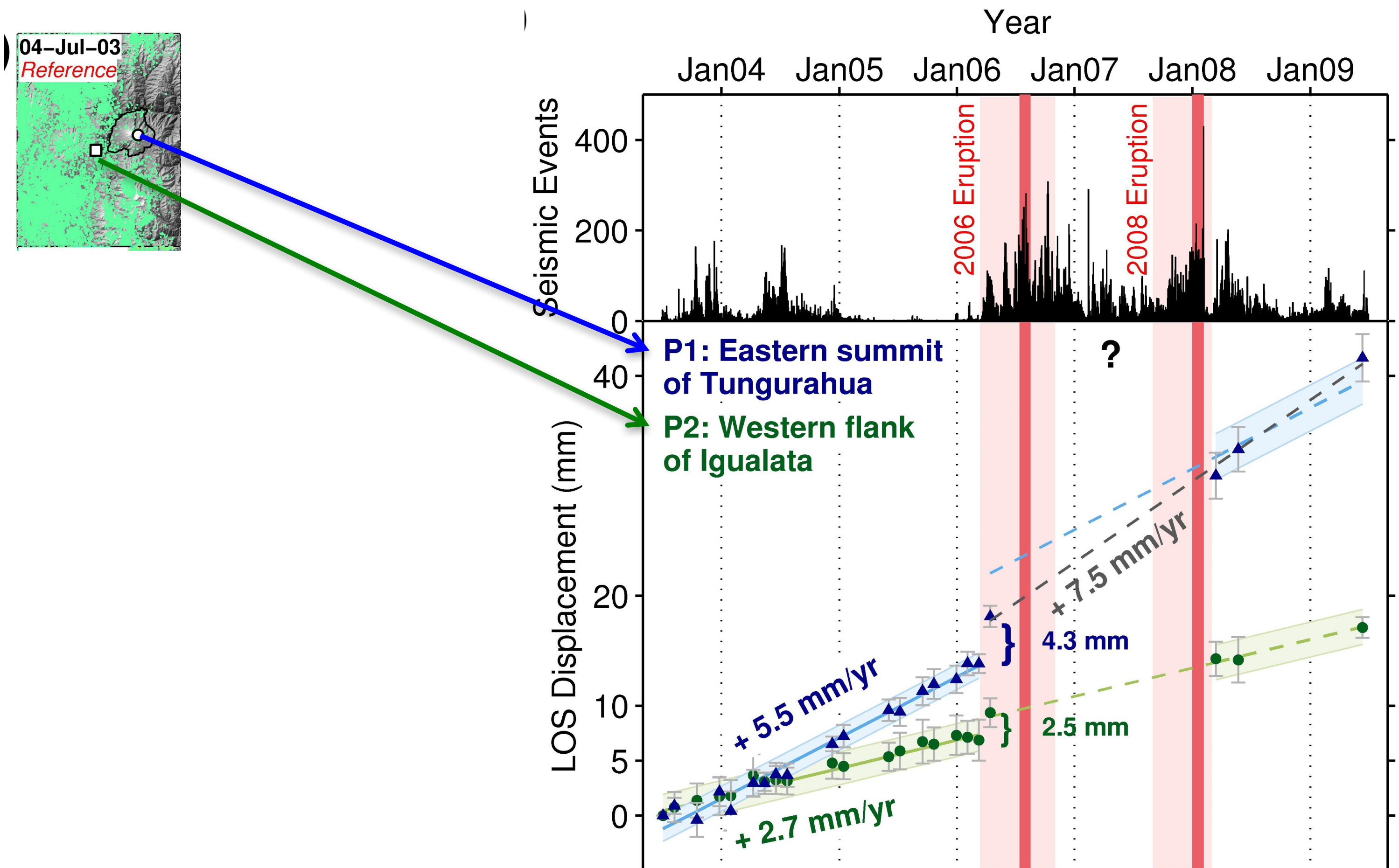

1. ≈ Constant uplift rate
2. Offset prior to the 2006 eruption

Modelled source for the constant inflation rate

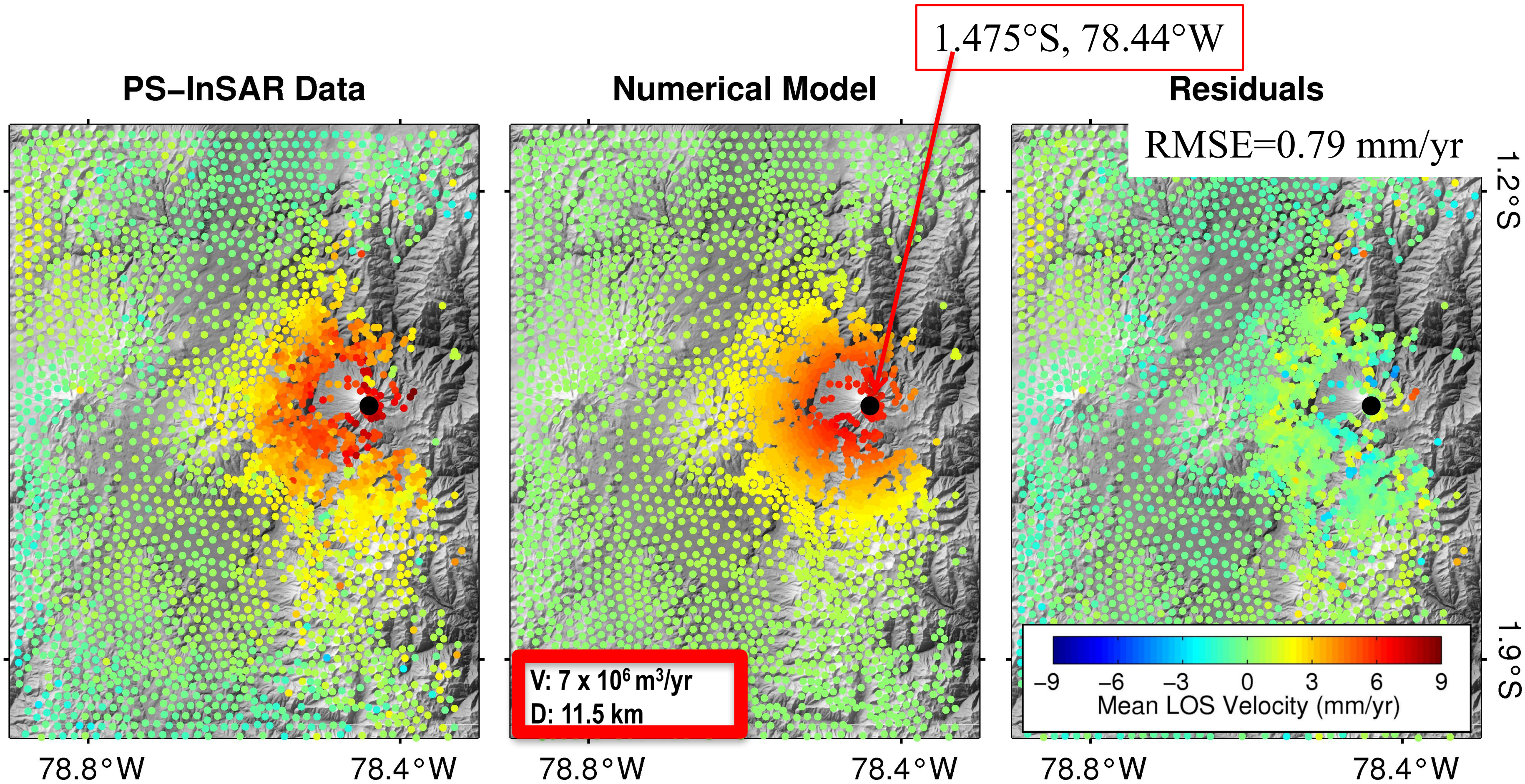

A storage zone at 11.5 km below sea level in good agreement with petrological data

Temporal evolution

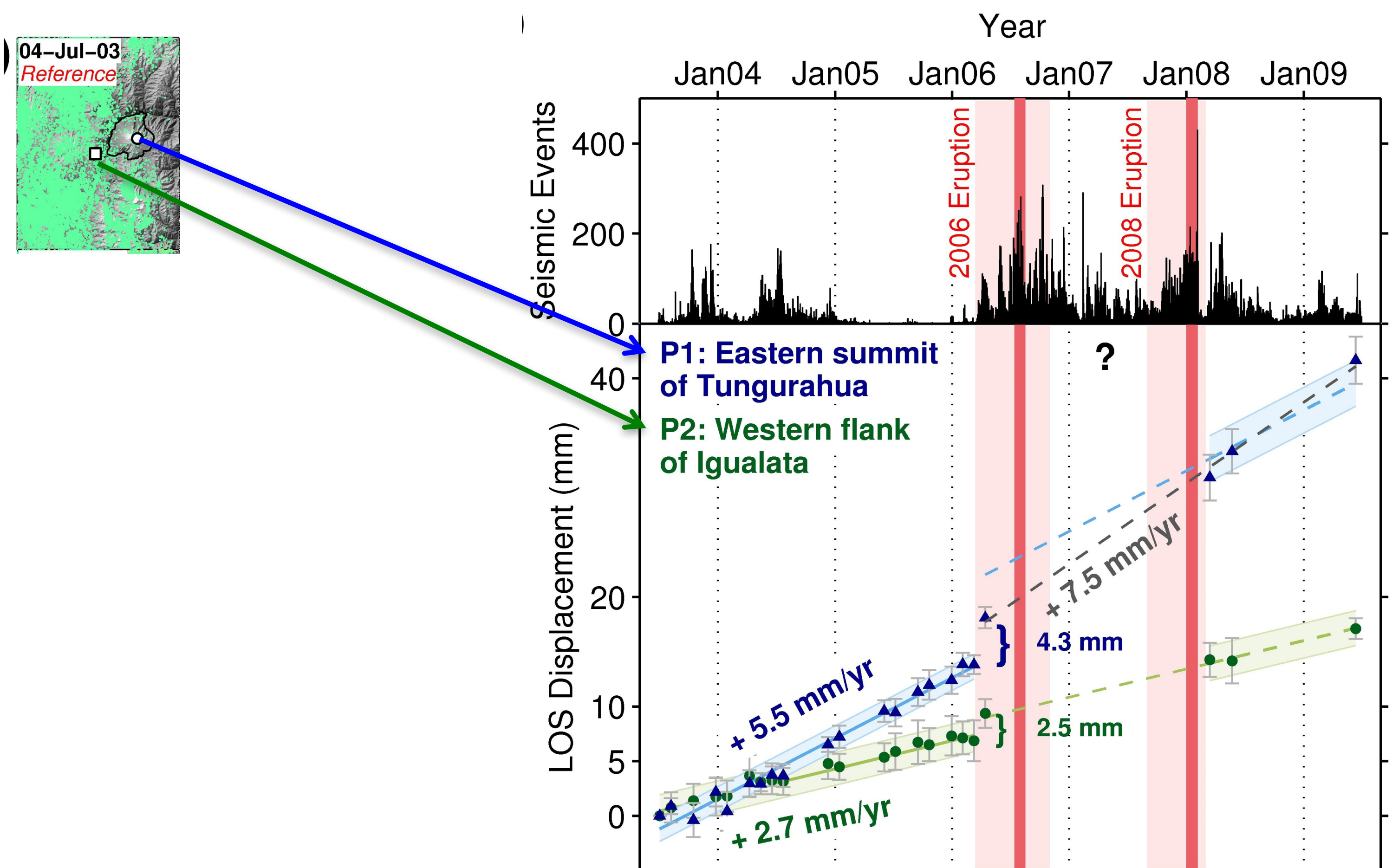

2. Offset prior to the 2006 eruption
Modelled with the same source and an additional volume of magma (4.5 million of m^3)

What we learned…

*For the Tungurahua plumbing system:

Emplacement of at least 7 million of m^3/yr at 11.5 km below sea level

Additional inflow of 4.5 million of m^3 prior to the 2006 eruption
Possibly induced the eruption

Good agreement with petrological data

→On the studied period: 46.5 million of m^3 emplaced at depth
30 million of m^3 of magma (DRE) erupted

*More generally:

First evidence of long-term (6 years) inflation for a volcano in current activity in the Andes

➔ **Magma erupted is compensated at depth by an acceleration of magma input**

Deformation/volcanic activity in the Andes as revealed by InSAR

Eruption
No deformation detected by InSAR

Nevado del Huila Colombia
Guagua Pichincha, Ecuador
Ubinas, Peru
Irruputuncu, Chile
Planchon Peteroa, Chile
Villarica, Chile

No eruption
Long-term inflation

Hualca Hualca, Peru
Uturuncu, Bolivia
Lazufre, Chile-Argentina
Laguna del Maule, Chile

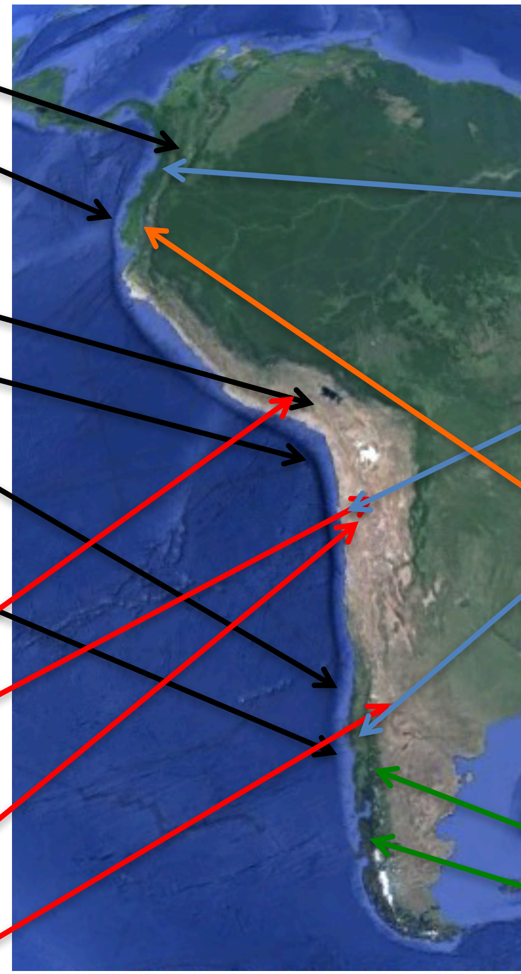

Eruption
Co or post-eruptive deformation

Galeras, Colombia
Lascar, Chile
Llaima, Chile

In eruption
Long-term inflation

Tungurahua, Ecuador

Eruption
Pre-eruptive inflation

Cordon Caulle, Chile
Cerro Hudson, Chile

From Biggs et al, 2014

SAR application summary

- Production of surface displacement field maps:
  - Earthquakes (co-seismic)
  - Inter-seismic loading on faults
  - Landslides
  - Volcanoes
  - *Subsidence in urban areas*
- DEM production
- Detection of surface changes
  - Estimation of post-event damages
  - Mapping of eruptive deposits

Anthropogenic hazards (subsidence due to mining operations or fluid extraction/injection)

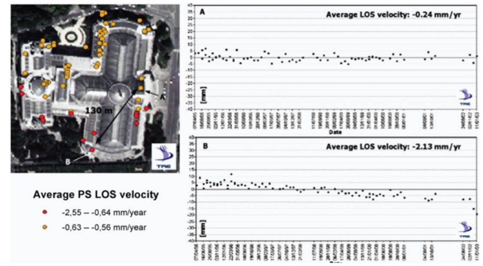

Deformation on the Grand Palais (Paris) between 1995 and 2003, seen through PSI interferometry (Raucoules et al., 2007 – processing TRE). The south wing subsides at a rate of 2mm/yr, while the north wing is stable throughout the monitored period. Time Series of the deformation in the Line of Sight of two significant PSs (A and B) are shown.

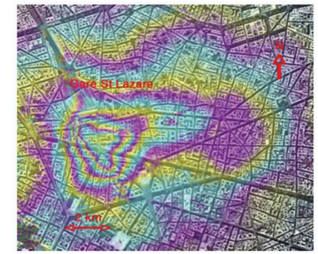

Vertical movement (soil heave) related to work on the Paris metro in July 1998 (Raucoules et al., 2007; after Le Mouélic et al., 2002)

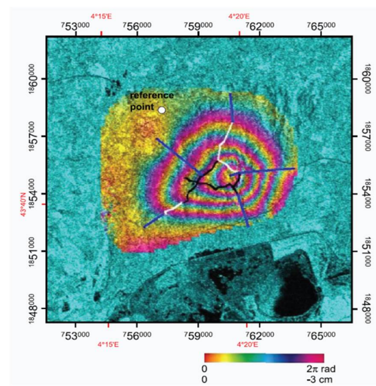

Subsidence related to salt mining in Vauvert (after Raucoules et al., 2003) over the period 1993-1999.

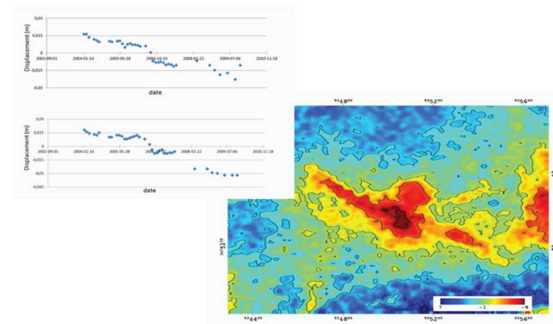

Subsidence related to dissolution of salt in the municipality of Hilsprich (after Raucoules et al., 2013). Stack of PALSAR interferograms and ASAR Time Series on some PS points on the edge of a subsidence basin..

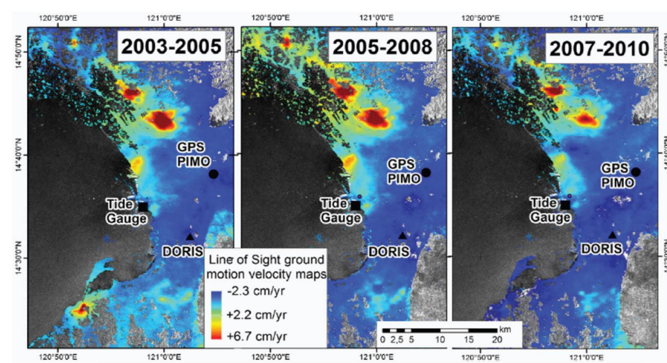

Deformations in urban Manila related to over-exploitation of groundwater (after Raucoules et al., 2013)

<u>From Pinel and Raucoules, 2016</u>

Anthropogenic hazards (subsidence due to mining operations or fluid extraction/injection)

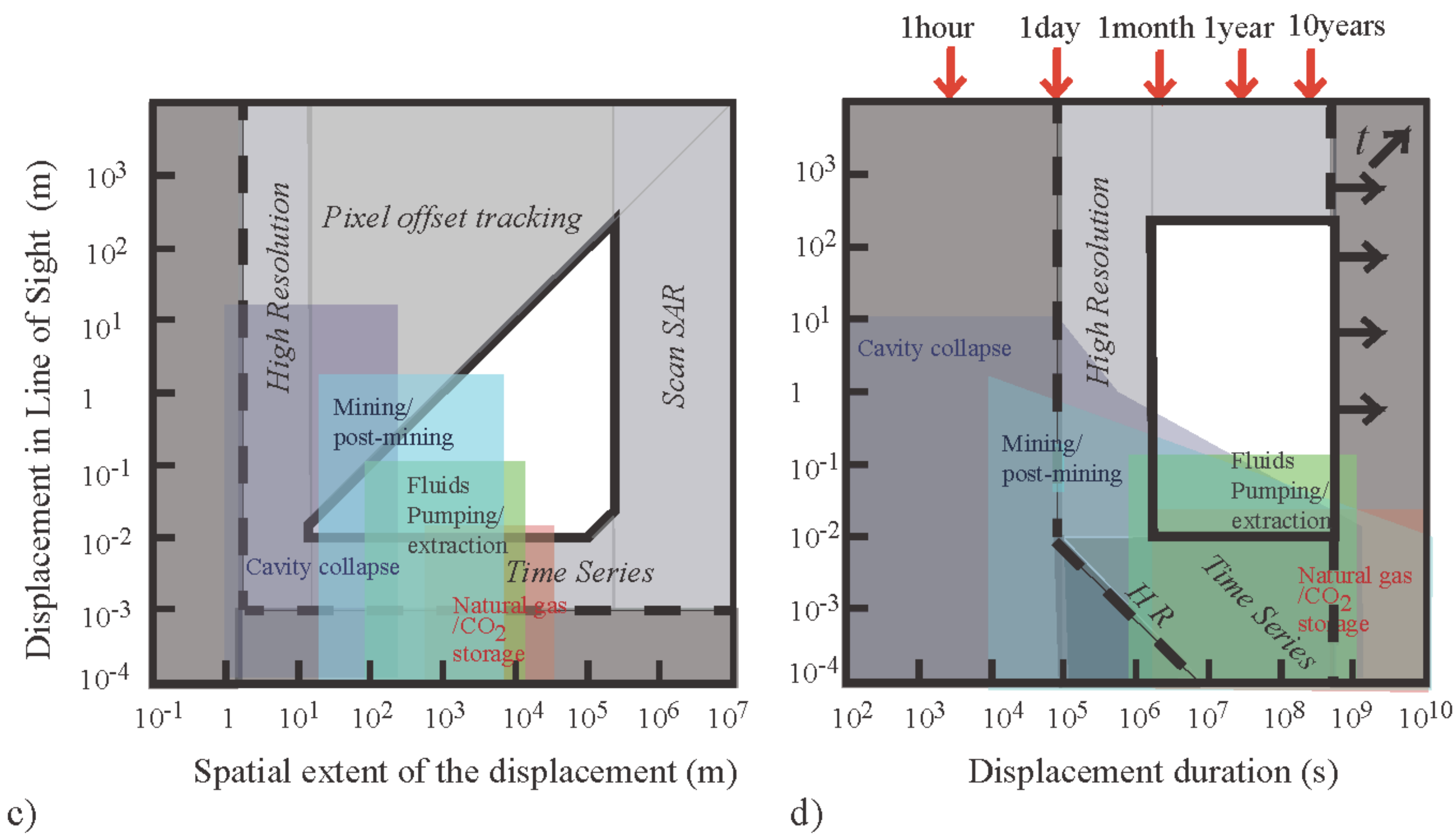

From Pinel and Raucoules, 2016

Anthropogenic hazards (Mexico city subsidence)

Mexico City location

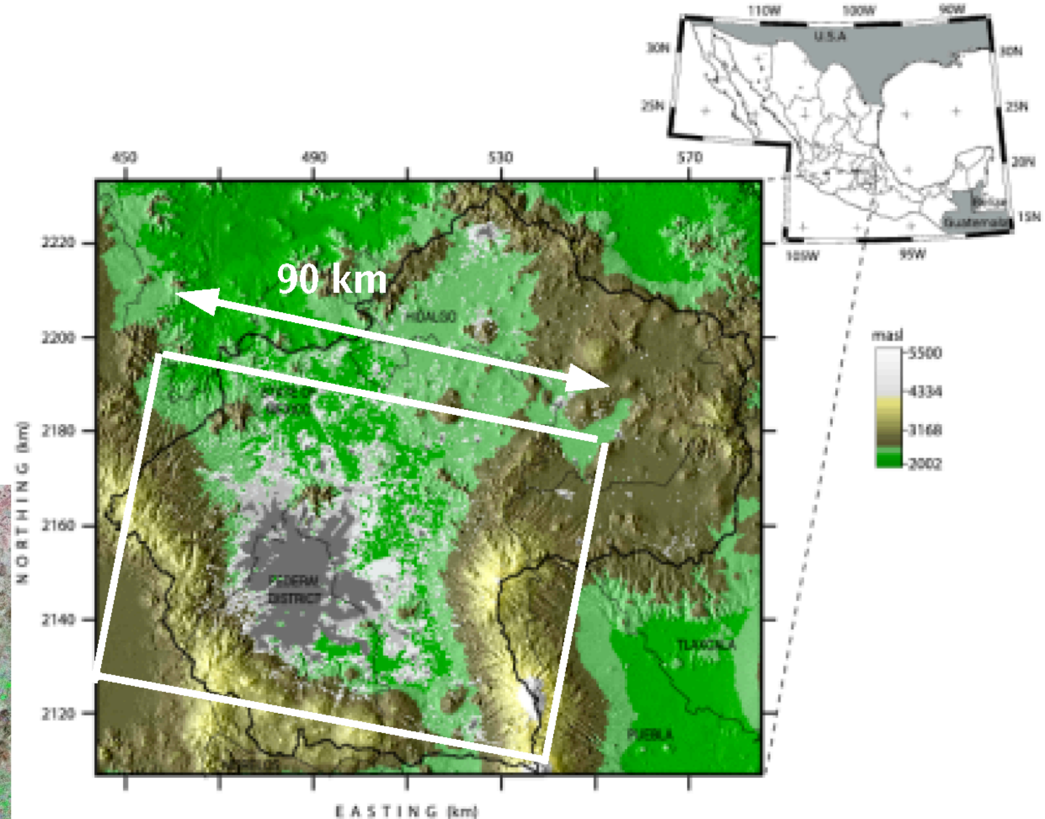

Landsat

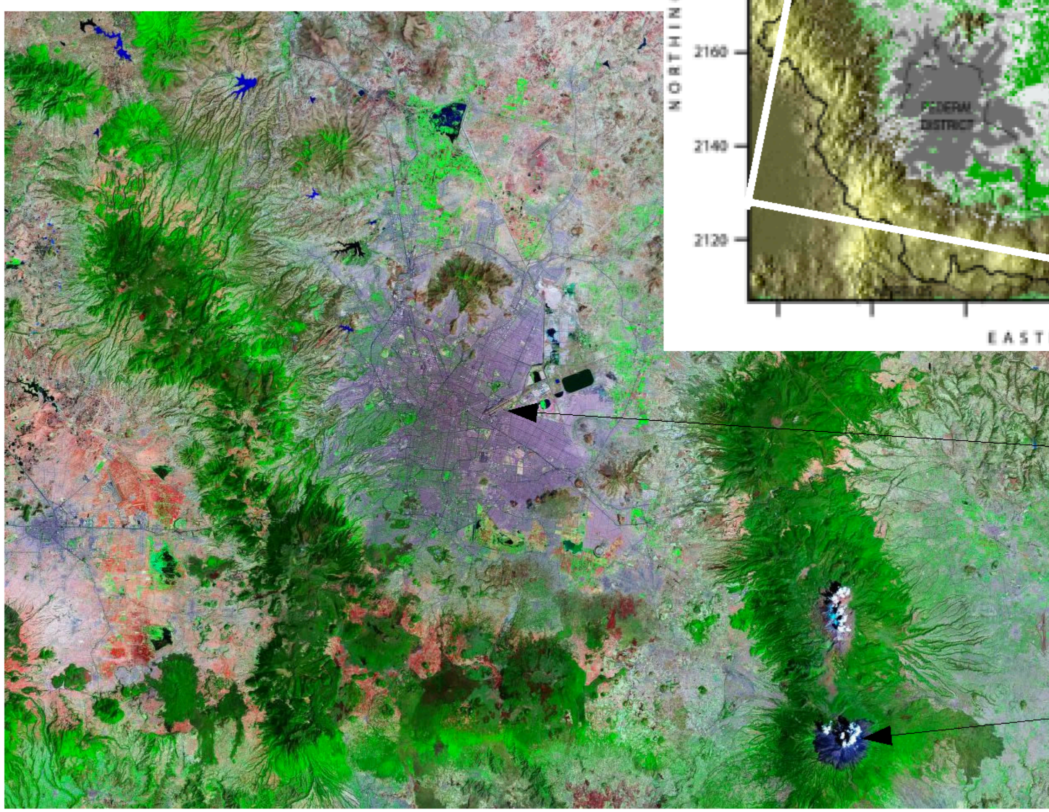

Airport

Popocatepelt

From Doin et al, 2010

Anthropogenic hazards (Mexico city subsidence)

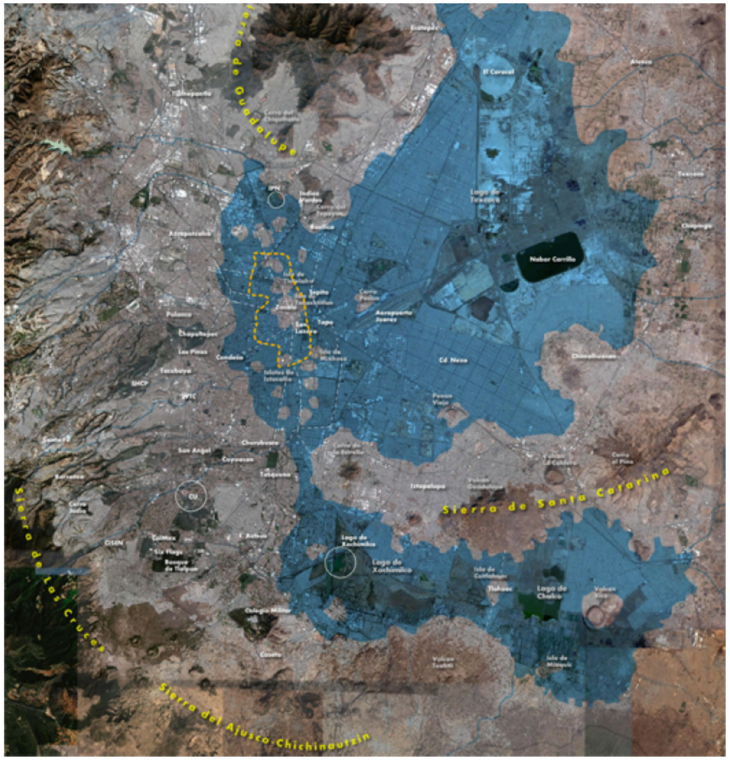

Former lake (before spanish conquest)

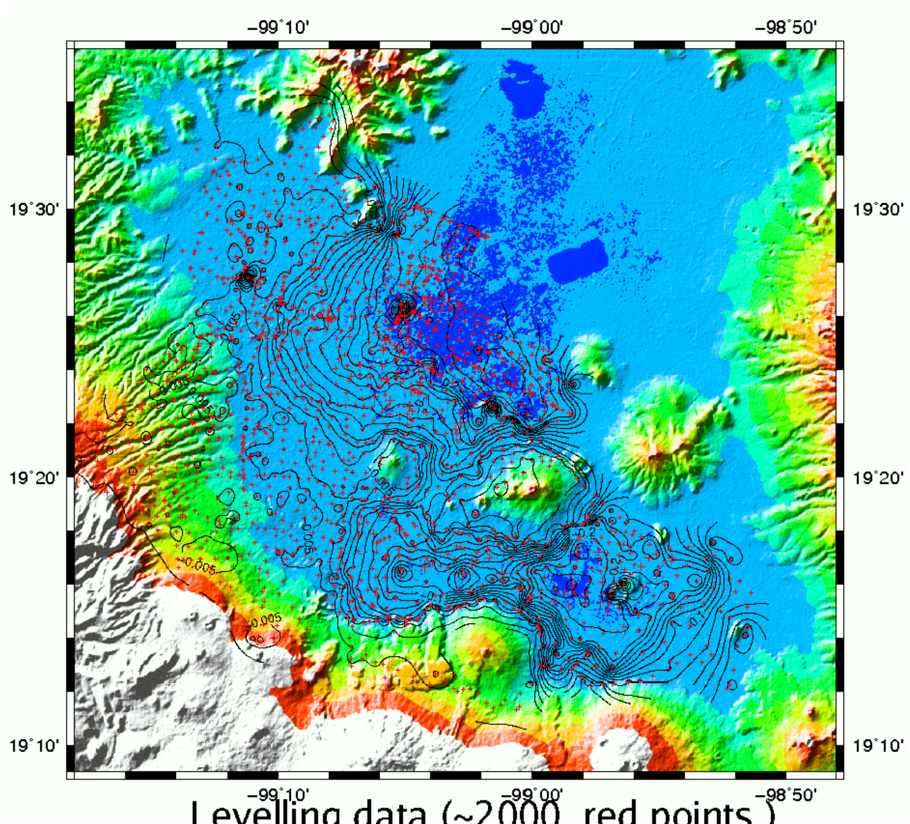

Levelling data (~2000, red points)

Comision Nacional del Agua

Compaction of the lacustrine clay layer following the water level drawdown in the underlying aquifer

Maximum = 38 cm/yr Two main subsiding areas; volcanoes (small or large) in and out the city do not subside

From Doin et al, 2010

Anthropogenic hazards (Mexico city subsidence)

- Temporal analysis of 38 Envisat acquisitions between end of 2002 and the beginning of 2007 :

  SBAS (« Small BAseline Subset ») : home-made software
  PS : Gamma IPTA
  StaMPS : version SB

- SAR image correlation during the period 1995-2007

- Levelling data from the Comision National del Agua

From Doin et al, 2010

Anthropogenic hazards (Mexico city subsidence)

Example of an interferogram at 9 x 35 days :

$$\Phi_{ij}^{diff} = \varphi_{res\text{-}orb} + \varphi_{res\text{-}MNT} + \varphi_{atm}\,(j\text{-}i) + \varphi_{def}(j\text{-}i) + \text{decorrelation noise}$$

Spatial unwrapping very difficult !
Strong temporal decorrelation in vegetated areas

2004 01 16–2004 11 26

$B_{\perp}$ = 265 m

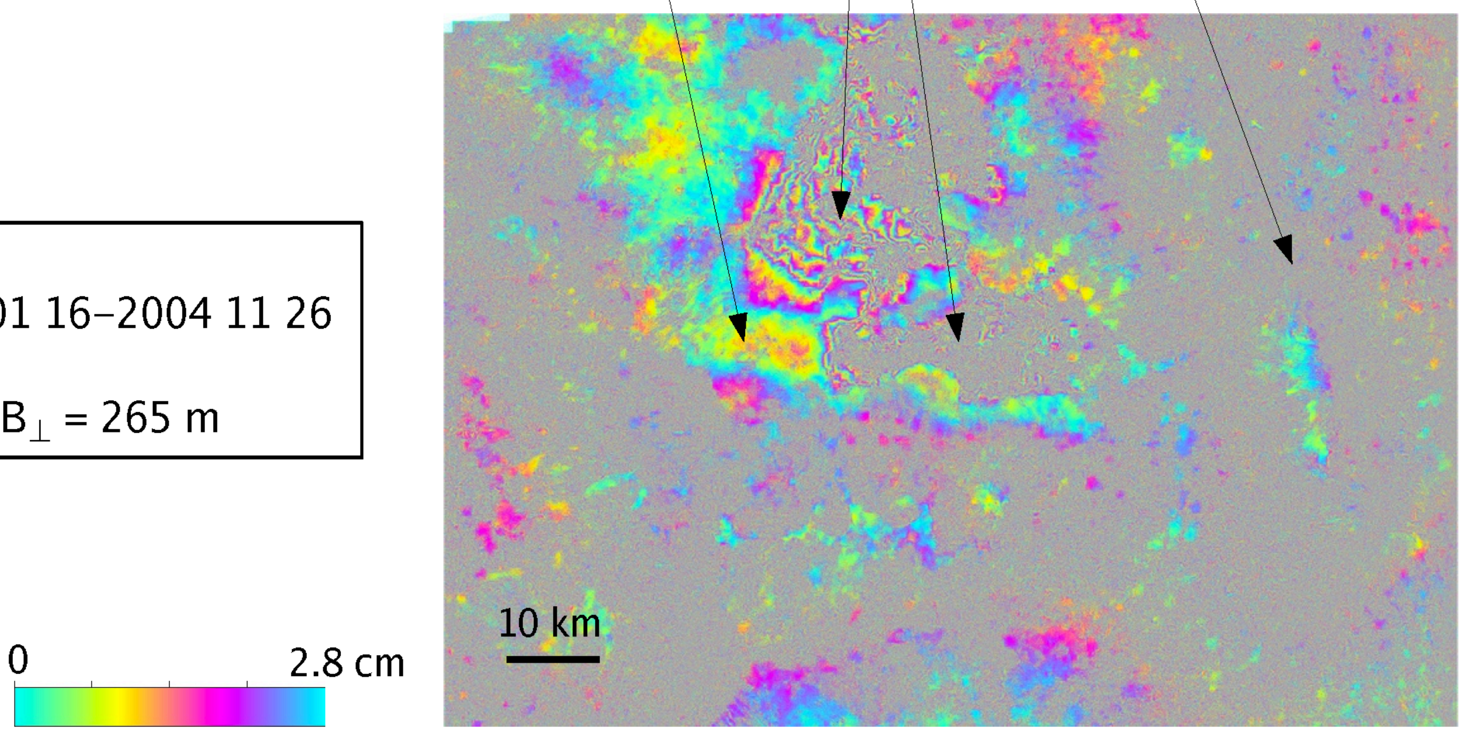

From Doin et al, 2010

Anthropogenic hazards (Mexico city subsidence)

I –« SBAS » temporal analysis

Network of small baseline interferograms with redundancy

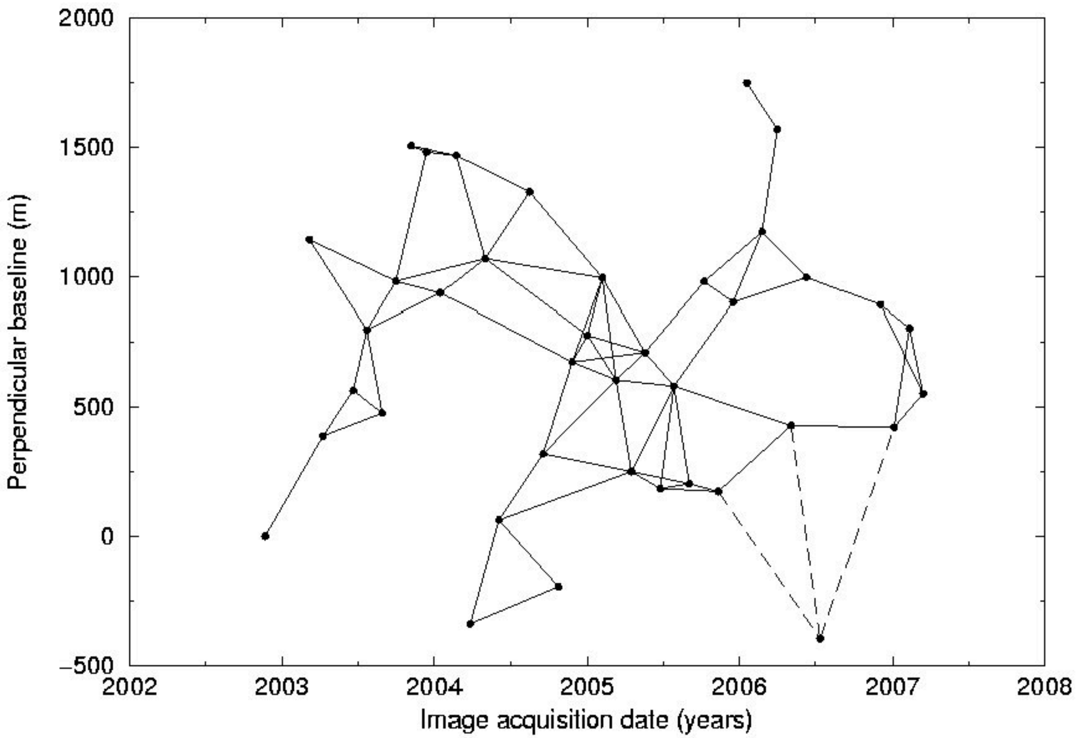

71 interferograms
38 ENVISAT scenes

$B_\perp < 500$ m
$\Delta t < 10$ months

Cavalié et al., J. Geophysical Research, 2007
P. Lopez-Quiroz, PhD thesis, 2008
Lopez-Quiroz et al., J. of Applied Geophysics, 2009

From Doin et al, 2010

Anthropogenic hazards (Mexico city subsidence)

Spatial unwrapping strategy : remove filtered stack from wrapped interferograms

- Stack of 5 very well unwrapped interferograms at 35 or 70 jours
- Filtered to remove decorrelation noise
- Uncertainty : about a few cm/yr

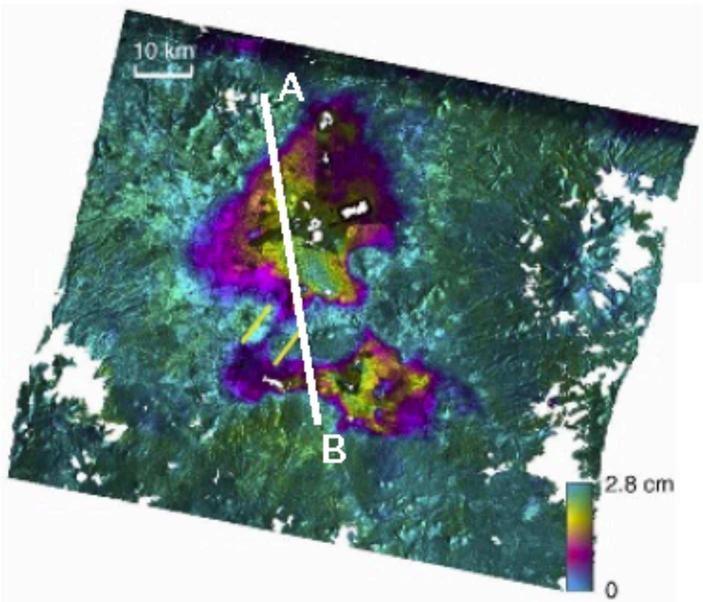

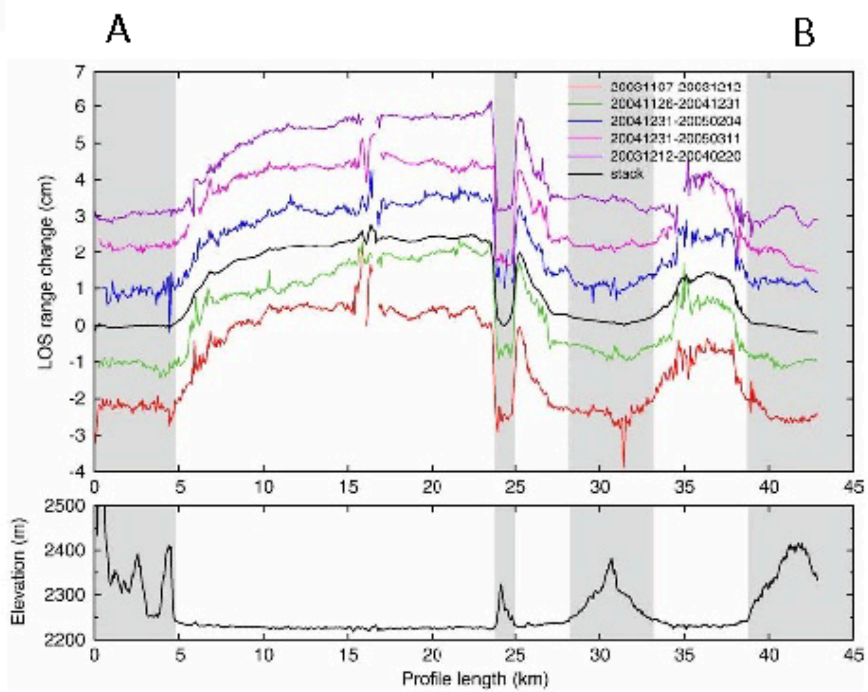

Subsidence profiles in 35 days:
- extreme gradients
- volcanoes do not subside

From Doin et al, 2010

Anthropogenic hazards (Mexico city subsidence)

Closure of the interferometric network

$$RMS = \sum(\Phi_{ij} - \sum_{k=i}^{j-1} d\varphi_k)^2$$

- Decorrelation noise

- <u>Unwrapping errors</u>
  si RMS > 0.15 cm
  < 5% des pixels

From Doin et al, 2010

Anthropogenic hazards (Mexico city subsidence)

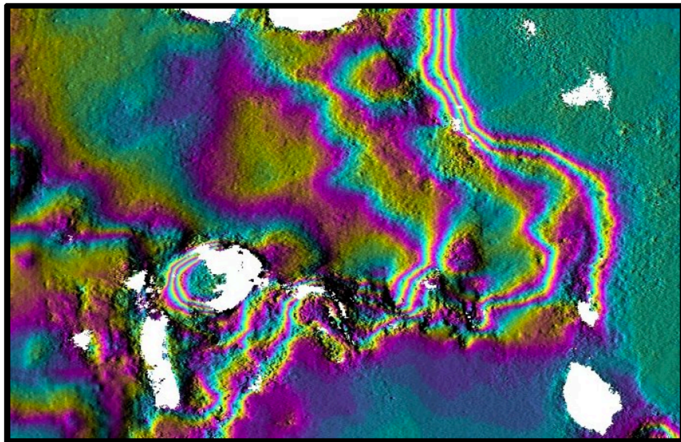

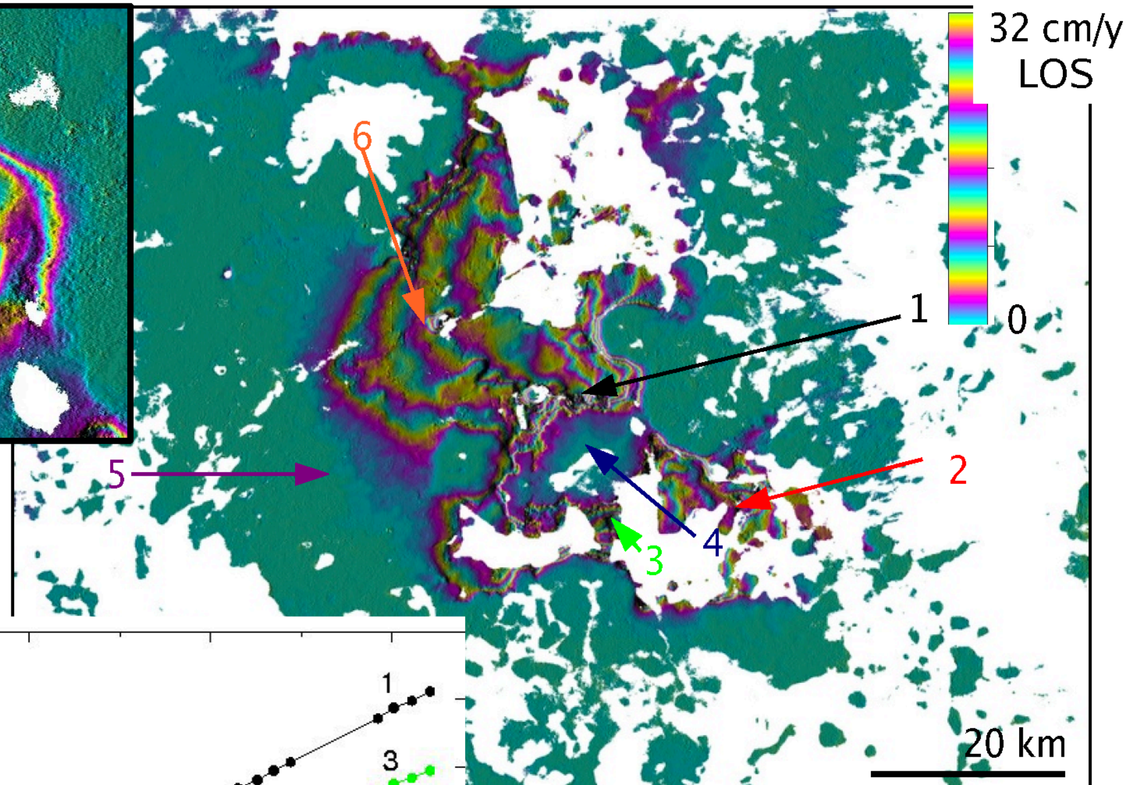

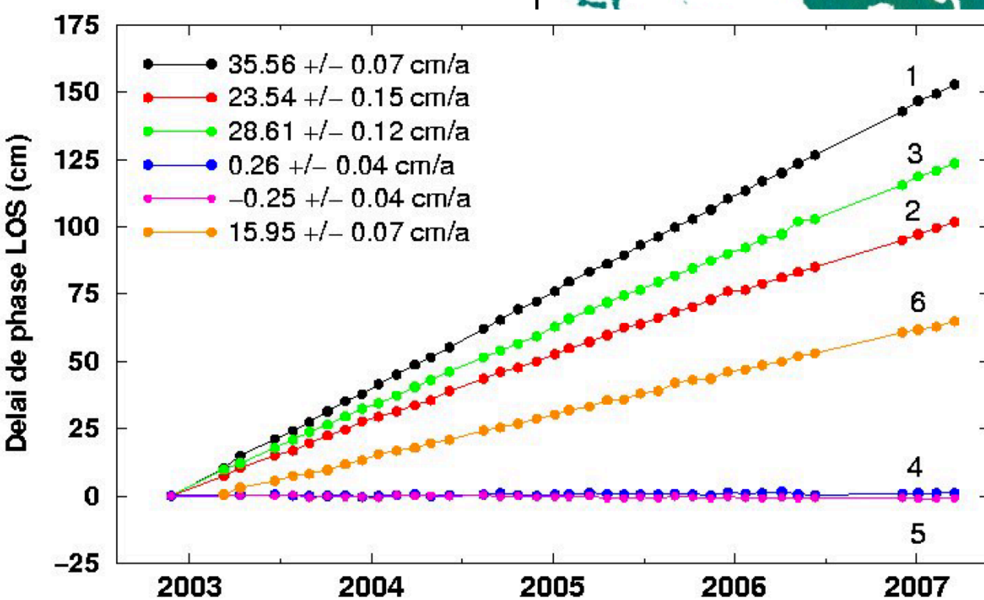

Average subsidence rate

From Doin et al, 2010

Anthropogenic hazards (Mexico city subsidence)

$$\varphi_m = e\, B_\perp{}^m + a\,(t_m - t_1) + b\,(t_m - t_1)^2 + c + APS_m$$

Acceleration (blue areas) or deceleration (red areas) of subsidence

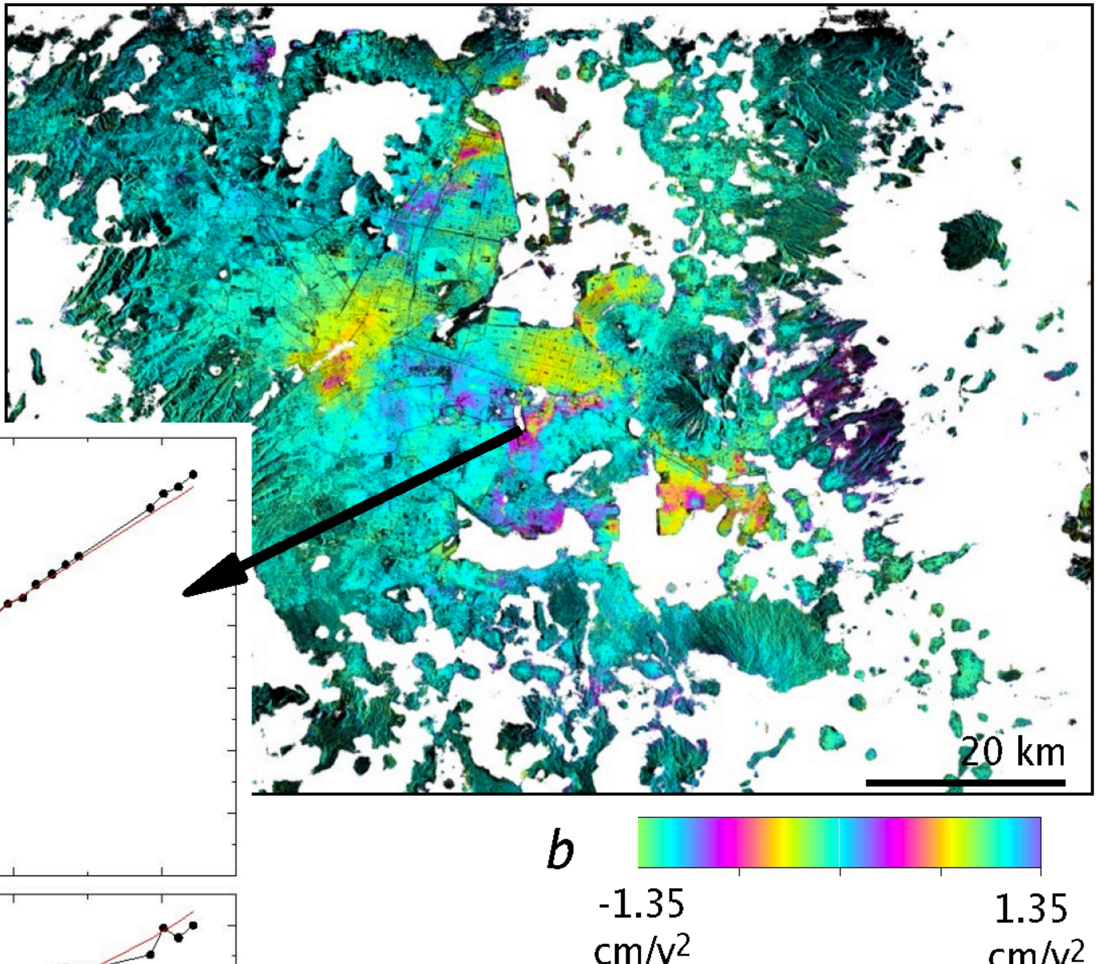

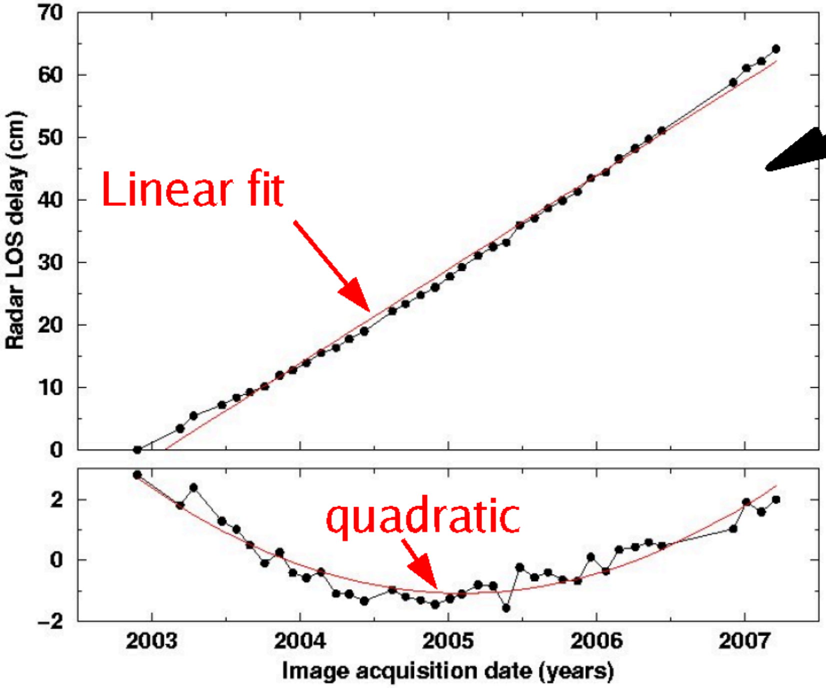

From Doin et al, 2010